LETTER

doi:10.1038/nature22078

Polyglutamine tracts regulate beclin 1–dependent autophagy

Avraham Ashkenazi[1], Carla F. Bento[1], Thomas Ricketts[1], Mariella Vicinanza[1], Farah Siddiqi[1], Mariana Pavel[1], Ferdinando Squitieri[2], Maarten C. Hardenberg[1], Sara Imarisio[1], Fiona M. Menzies[1] & David C. Rubinsztein[1]

Nine neurodegenerative diseases are caused by expanded polyglutamine (polyQ) tracts in different proteins, such as huntingtin in Huntington's disease and ataxin 3 in spinocerebellar ataxia type 3 (SCA3)[1,2]. Age at onset of disease decreases with increasing polyglutamine length in these proteins and the normal length also varies[3]. PolyQ expansions drive pathogenesis in these diseases, as isolated polyQ tracts are toxic, and an N-terminal huntingtin fragment comprising exon 1, which occurs *in vivo* as a result of alternative splicing[4], causes toxicity. Although such mutant proteins are prone to aggregation[5], toxicity is also associated with soluble forms of the proteins[6]. The function of the polyQ tracts in many normal cytoplasmic proteins is unclear. One such protein is the deubiquitinating enzyme ataxin 3 (refs 7, 8), which is widely expressed in the brain[9,10]. Here we show that the polyQ domain enables wild-type ataxin 3 to interact with beclin 1, a key initiator of autophagy[11]. This interaction allows the deubiquitinase activity of ataxin 3 to protect beclin 1 from proteasome-mediated degradation and thereby enables autophagy. Starvation-induced autophagy, which is regulated by beclin 1, was particularly inhibited in ataxin-3-depleted human cell lines and mouse primary neurons, and *in vivo* in mice. This activity of ataxin 3 and its polyQ-mediated interaction with beclin 1 was competed for by other soluble proteins with polyQ tracts in a length-dependent fashion. This competition resulted in impairment of starvation-induced autophagy in cells expressing mutant huntingtin exon 1, and this impairment was recapitulated in the brains of a mouse model of Huntington's disease and in cells from patients. A similar phenomenon was also seen with other polyQ disease proteins, including mutant ataxin 3 itself. Our data thus describe a specific function for a wild-type polyQ tract that is abrogated by a competing longer polyQ mutation in a disease protein, and identify a deleterious function of such mutations distinct from their propensity to aggregate.

The induction of autophagy enhances the clearance of polyQ-expanded proteins, such as mutant huntingtin and ataxin 3, and thereby attenuates their toxicity[5,12,13]. To understand the interplay between polyQ-containing proteins and autophagy, we investigated whether wild-type ataxin 3 affected this process. Conjugation of the autophagy protein LC3-I (the mammalian Atg8 orthologue also known as Map1lc3b) to phosphatidylethanolamine on autophagosomal membranes forms LC3-II. Hence, LC3-II levels (relative to loading controls such as actin) correlate with autophagosome load[14–16]. Ataxin 3 knockdown in mouse primary neurons (Fig. 1a) using a short hairpin RNA (shRNA) targeting *Atxn3* lowered LC3-II levels in the presence of bafilomycin A1 (BafA1). As BafA1 inhibits LC3-II degradation, this result suggests that ataxin 3 knockdown impaired autophagosome synthesis. Decreased levels of LC3-II (but not LC3-I) were also observed in ataxin-3-depleted, BafA1-treated neurons in starvation medium (Fig. 1b, Extended Data Fig. 1a). Moreover, ataxin 3 knockdown in HeLa cells reduced the level of LC3-II and increased the level of the autophagy substrate, p62 (Extended Data Fig. 1b, c). Ataxin 3 knockdown decreased the number of autophagosomes and autolysosomes scored with the reporter mTagRFP–mWasabi–LC3, consistent with impaired autophagosome formation (Extended Data Fig. 1d).

The decrease in autophagosome biogenesis following ataxin 3 knockdown was associated with a decrease in beclin 1 (Fig. 1c). The phosphatidylinositol 3-phosphate (PtdIns3P) formed by the complex between beclin 1 and the phosphatidylinositol 3 kinase VPS34 is particularly important for inducing autophagy (LC3-II formation in BafA1-treated cells) after nutrient depletion, and such defects are seen in cells with monoallelic deletion of the gene encoding beclin 1 (*becn1*)[11,17,18]. Ataxin-3-depleted cells cultured in starvation medium showed a decrease in PtdIns3P-positive structures, characteristic of beclin 1-depletion[18] (Extended Data Fig. 1e). In both fed and starved conditions, loading back exogenous PtdIns3P to ataxin-3-depleted cells increased LC3 vesicle numbers to levels comparable to control cells (Extended Data Fig. 2a, b). Ataxin 3 overexpression increased the number of puncta positive for the PtdIns3P-binding autophagy effector WIPI2, which binds to PtdIns3P at autophagy initiation membranes[19,20]. This effect was reversed when ataxin 3 overexpressing cells were treated with the phosphatidylinositol 3 kinase inhibitor wortmannin (Extended Data Fig. 2c). After mice were starved, livers depleted of ataxin 3 failed to upregulate beclin 1 or LC3-II (Fig. 1d, e, Extended Data Fig. 2d) and showed increased p62 levels (Extended Data Fig. 2e, f), compared to wild-type livers. Therefore, ataxin 3 knockdown decreased beclin 1 levels, which could explain the decrease in PtdIns3P and consequent impairment in autophagosome biogenesis.

As ataxin 3 interacted with beclin 1 (Fig. 2a), we tested whether the deubiquitinase activity of ataxin 3 protected beclin 1 against proteasomal degradation. Beclin 1 levels declined more in ataxin-3-depleted cells than in controls after inhibition of protein synthesis, suggesting that depletion of ataxin 3 accelerated beclin 1 turnover (Extended Data Fig. 3a). Beclin 1 levels were restored in ataxin 3 knockdown cells treated with a proteasome inhibitor (Extended Data Fig. 3b) and when ataxin-3-depleted cells were transfected with wild-type ataxin 3 but not with a ubiquitin protease-dead mutant (C14A; Extended Data Fig. 3c). Under proteasome inhibition, ubiquitination of endogenous beclin 1 was increased when ataxin 3 was knocked down (Extended Data Fig. 3d), and recombinant ataxin 3 but not the protease-dead C14A mutant deubiquitinated beclin 1 *in vitro* (Fig. 2b, Extended Data Fig. 3e, f showing beclin 1 selectivity). The percentage of cells containing mutant huntingtin exon 1 aggregates correlates with levels of this protein and decreases when autophagy is induced[12]. Consistent with autophagy induction, overexpression of wild-type (but not C14A) ataxin 3 decreased the percentage of such mutant huntingtin-expressing cells that contained aggregates (Extended Data Fig. 3g).

Our mass spectrometry analysis and others[21] suggest that lysine 402 of beclin 1 was modified with a lysine 48 (K48) ubiquitin chain, a

[1]Department of Medical Genetics, Cambridge Institute for Medical Research (CIMR), University of Cambridge, Cambridge, UK. [2]IRCCS Casa Sollievo della Sofferenza, Huntington and Rare Diseases Unit, San Giovanni Rotondo, Italy.

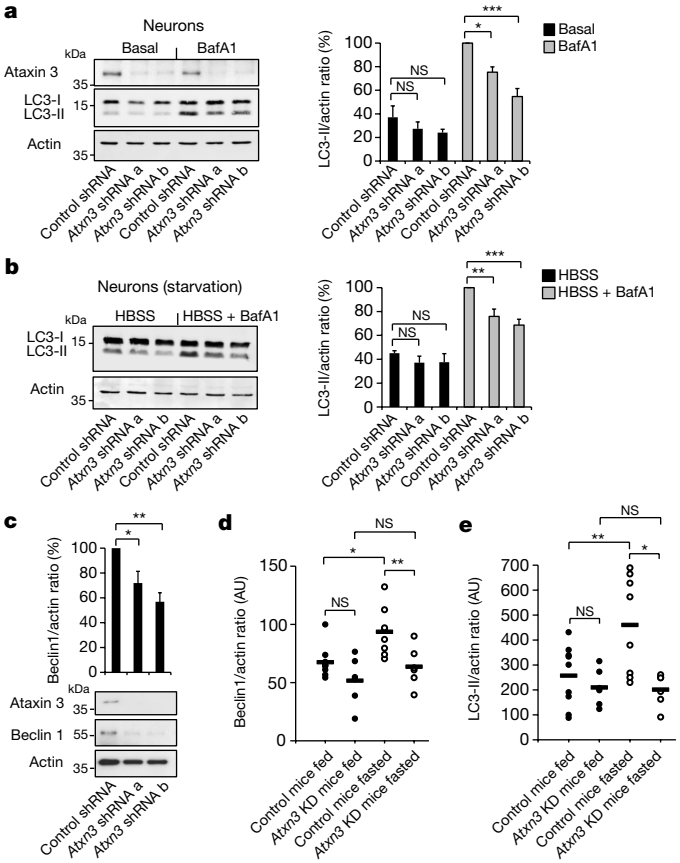

Figure 1 | Ataxin 3 contributes to autophagosome formation by regulating the levels of beclin 1. a–c, Mouse cortical neurons were transduced with control or *Atxn3*-targeting lentiviral shRNAs and analysed for LC3-II levels with or without BafA1 (**a**); LC3-II levels in starvation medium (HBSS) with or without BafA1 (**b**); and beclin 1 levels in the starved cells (**c**). Results are mean ± s.e.m; $n = 5$ replicates from two independent cultures. **d**, **e**, Control mice and mice depleted of liver ataxin 3 (*Atxn3* KD) were fed or starved for 24 h. Liver samples were analysed for beclin 1 (**d**) and LC3-II (**e**). Control fed $n = 9$, *Atxn3* knockdown fed $n = 6$, control fasted $n = 8$, *Atxn3* knockdown fasted $n = 6$. AU, arbitrary units. Extended statistical analysis in Supplementary Table 1. Two-way ANOVA with Bonferroni's post-test (**a**, **b**, **d**, **e**). One-way ANOVA with post hoc Tukey's test (**c**). $*P < 0.05$, $**P < 0.01$, $***P < 0.001$; NS, not significant. For representative blots and *in vivo* ataxin 3 knockdown efficiency, see Extended Data Fig. 2d. For gel source images see Supplementary Fig. 1.

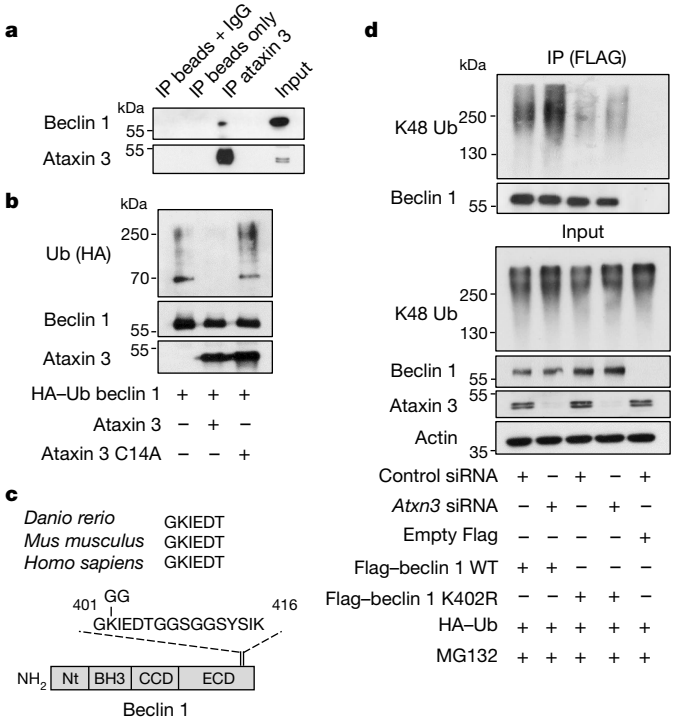

Figure 2 | Deubiquitination of beclin 1 by ataxin 3. a, Endogenous ataxin 3 was immunoprecipitated (IP) from HeLa cell lysates and blots probed for endogenous beclin 1 and ataxin 3. **b**, Ubiquitinated (Ub) beclin 1 was incubated *in vitro* with recombinant ataxin 3 or ataxin 3 C14A for 2 h and analysed for beclin 1 ubiquitination using anti-haemagglutinin (HA) antibodies. **c**, Evolutionary conservation of region around beclin 1 K402. **d**, Control and ataxin-3-depleted (*Atxn3* small inhibitory RNA (siRNA)) HeLa cells were transfected as indicated for 24 h and incubated for the last 6 h with the proteasome inhibitor MG132 (10 μM). Wild-type (WT) Flag-tagged beclin 1 and mutant Flag-tagged beclin 1 K402R were immunoprecipitated with anti-Flag antibodies for ubiquitination analysis. For gel source images see Supplementary Fig. 1.

signal for proteasomal degradation (Fig. 2c, Extended Data Fig. 4a, b). Lysine 402 in the evolutionary conserved domain (ECD) of beclin 1 is conserved in fish, mice and humans (Fig. 2c). K48-linked beclin 1 polyubiquitination was increased by depletion of ataxin 3, and mutation of lysine 402 to arginine (K402R) decreased K48-linked beclin 1 polyubiquitination, confirming that K402 is a site for this modification (Fig. 2d). Consequently, K402R beclin 1 was more abundant than wild-type beclin 1 in cells, and levels of K402 beclin 1 did not increase further after treatment with proteasome inhibitors (Extended Data Fig. 4c). Ataxin 3 expression in HeLa cells increased wild-type beclin 1 levels and did not increase levels of beclin 1 K402R (Extended Data Fig. 4d). This result is consistent with the finding that cells overexpressing K402R beclin 1 show more autophagy than those overexpressing the wild-type protein (Extended Data Fig. 4d).

Deletion of the polyQ domain from ataxin 3 greatly reduced its binding to beclin 1 (Fig. 3a), and an isolated polyQ stretch was sufficient to bind beclin 1 (Fig. 3b). Thus, the polyQ domain is important for the ataxin 3–beclin 1 interaction, but is not the only binding domain. The beclin l ECD interacted with ataxin 3 (Fig. 3c) and also bound the polyQ tract alone (Extended Data Fig. 5a), suggesting that the ECD of beclin 1 contained polyQ-binding domains, consistent with structural docking models revealing two highly scored polyQ-binding pockets in the beclin 1 ECD (Fig. 3d, Extended Data Fig. 5b–e). As some binding was observed with beclin 1 lacking the ECD, other domains of beclin 1 may also interact with ataxin 3.

GFP-tagged isolated polyQ tracts could bind to beclin 1, and longer stretches (Q81) bound beclin 1 more strongly than shorter tracts (Q35) (Fig. 4a). Remarkably, beclin 1 K48-polyubiquitination was increased in cells overexpressing GFP–Q35 compared with those expressing empty GFP, and was increased even further by GFP–Q81 overexpression (Fig. 4a), consistent with a model in which these constructs compete with the ataxin 3 polyQ stretch that enables binding and subsequent deubiquitination of beclin 1. Indeed, overexpression of GFP–polyQ constructs decreased ataxin 3–beclin 1 binding (Fig. 4b). GFP–Q35 (which does not aggregate under our conditions) decreased beclin 1 levels (Extended Data Fig. 6a), impaired starvation-induced autophagy (Extended Data Fig. 6a, d, e) and increased p62 levels in starved cells (Extended Data Fig. 6b). No change in the number of LC3-II vesicles was observed when the Q35 tract was expressed in beclin-1-depleted cells (Extended Data Fig. 6c–e) and the inhibitory effect of Q35 on beclin 1 levels and autophagy in beclin-1-expressing cells was reversed by ataxin 3 overexpression (Extended Data Fig. 6a), compatible with a model in which Q35 impairs the control of beclin 1 levels by ataxin 3.

A wild-type (Q17) huntingtin fragment (N-terminal 350 residues) bound to beclin 1, and this interaction was largely lost when the polyQ stretch was deleted (Extended Data Fig. 7a). Furthermore, mutant polyQ-expanded, full-length huntingtin competed with wild-type ataxin 3 for beclin 1 binding (Extended Data Fig. 7b). To test

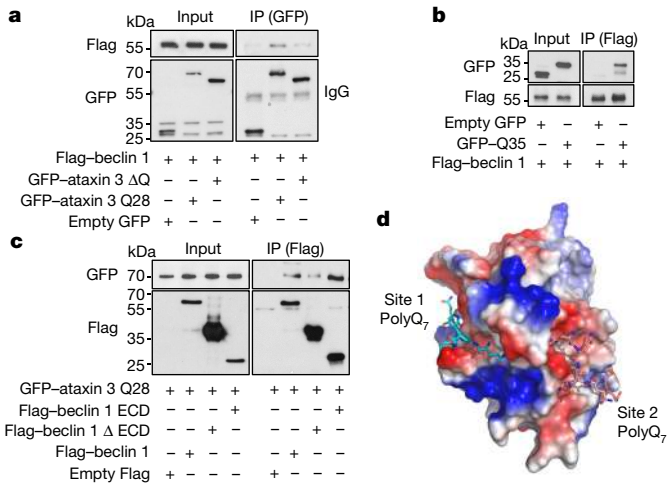

Figure 3 | The ataxin 3 polyQ domain contributes to the interaction between ataxin 3 and beclin 1. a–c, Constructs were transfected into HeLa cells for 24 h. **a**, Cell lysates were immunoprecipitated with anti-GFP antibodies and immunocomplexes analysed with anti-Flag antibodies. **b**, **c**, Cell lysates were immunoprecipitated with anti-Flag antibodies and immunocomplexes analysed with anti-GFP antibodies. For gel source images, see Supplementary Fig. 1. **d**, Structural docking modelling reveals two interaction sites between beclin 1 ECD and polyQ$_7$. Surface charge illustration of human beclin 1 ECD showing high-scored docking pose of polyQ$_7$ stretch (docking scores for site 1 and site 2 are −10.394 and −10.721, respectively). For full structural analysis see Extended Data Fig. 5.

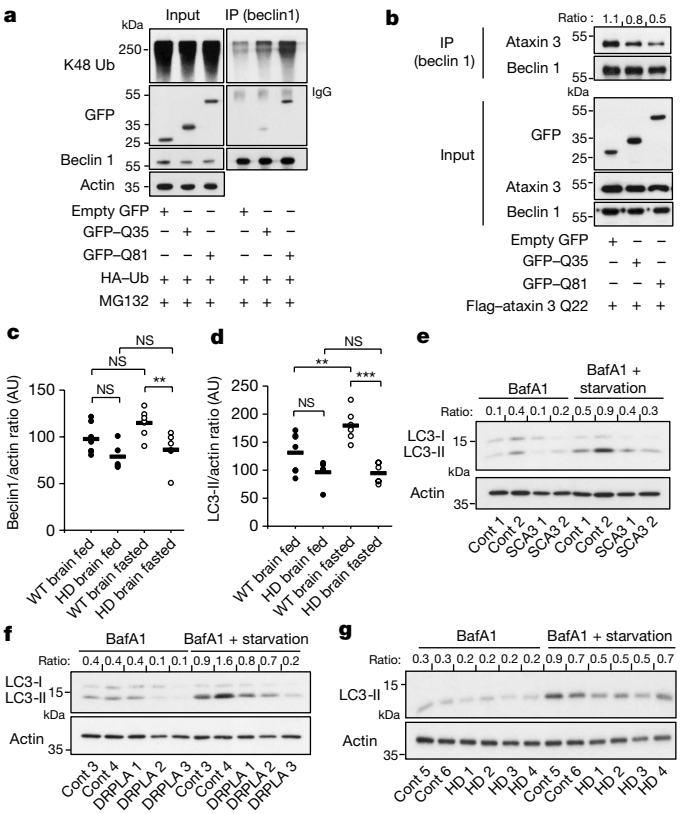

Figure 4 | Expanded polyQ tracts inhibit ataxin 3–beclin 1 interaction, decrease beclin 1 levels and impair starvation-induced autophagy. **a**, **b**, HeLa cells were transfected with indicated constructs for 24 h and immunoprecipitated for endogenous beclin 1. **a**, Cells treated for the last 6 h with proteasome inhibitor (MG132, 10 μM) were analysed for beclin 1 ubiquitination and for beclin 1-bound polyQ using anti-GFP antibodies. **b**, Immunocomplexes were analysed for beclin 1-bound ataxin 3 using anti-Flag antibodies. The bound ataxin 3/beclin 1 ratio is shown at the top. **c**, **d**, Brain samples from wild-type (WT) mice and Huntington's disease (HD) model transgenic mice were analysed for beclin 1 (**c**) and LC3-II (**d**). WT fed $n = 7$, HD fed $n = 5$, WT fasted $n = 7$, HD fasted $n = 6$; AU, arbitrary units. Extended statistical analysis in Supplementary Table 1. Two-way ANOVA with Bonferroni's post-test. Representative blots in Extended Data Fig. 8e. $^{**}P < 0.01$, $^{***}P < 0.001$; NS, not significant. **e–g**, Primary fibroblasts from healthy controls (Cont) or patients with different polyQ diseases (SCA3, DRPLA or HD (Huntington's disease)) treated with BafA1, in full or starvation medium analysed for LC3-II/actin ratio. For gel source images, see Supplementary Fig. 1.

the general principle on autophagy, we used an N-terminal exon 1 fragment to exclude any confounding effects of the huntingtin C terminus on autophagy[22]. In stable-inducible HEK293 cells expressing wild-type (Q23) and mutant (Q74) huntingtin exon 1 at similar levels (where there was no overt toxicity or aggregation (<1%) during the experiment), we observed lower beclin 1 levels and impaired starvation-induced autophagy after switching on the huntingtin transgene (Extended Data Fig. 7c–e). These effects were more pronounced in cells expressing the Q74 mutant. As these phenomena occur in both wild-type Q23-huntingtin-expressing cells and Q35-expressing cells, they cannot be explained simply by sequestration of beclin 1 into aggregates[23].

Next, we studied cell lines derived from the striatum, the brain region most sensitive to the Huntington's disease mutation, from heterozygous mutant huntingtin (Q7/Q111) and matched wild-type huntingtin knock-in mice (Q7/Q7) both humanized for huntingtin exon 1 (ref. 24). Mutant huntingtin (Q7/Q111) striatum-derived cells had lower beclin 1 levels and defects in starvation-induction of WIPI2 puncta and LC3-II levels, compared to wild-type (Q7/Q7) cells (Extended Data Fig. 8a–c). Likewise, brains from young mutant huntingtin exon 1 transgenic mice, in which there is minimal overt aggregation (Extended Data Fig. 8d), showed decreased beclin 1 levels in starving conditions, failed to upregulate LC3-II under starvation, and had increased p62 levels compared to wild-type littermate brains (Fig. 4c, d, Extended Data Fig. 8e–g).

We then tested whether this mechanism applied to mutant ataxin 3, as decreased beclin 1 levels are seen in rodent models of SCA3 (ref. 25). Expansion of the polyQ domain in ataxin 3 decreased its deubiquitinase activity towards beclin 1 (Extended Data Fig. 9a). Transfecting expanded ataxin 3 Q84 into ataxin 3 knockdown cells partially rescued the number of LC3 puncta but was not as effective as wild-type ataxin 3 Q28 (Extended Data Fig. 9b, c), consistent with the decreased deubiquitinase activity of the mutant protein. However, the polyQ-deleted ataxin 3 did not rescue the number of LC3 puncta (Extended Data Fig. 9b, c). When overexpressed in cells, Q84 mutant ataxin 3 interacted more strongly with beclin 1 than did wild-type ataxin 3, and this increased interaction was associated with increased beclin 1 K48 polyubiquitination, while no obvious change was observed in beclin 1 K63 polyubiquitination (Extended Data Fig. 9d). Thus, the longer polyQ stretches in mutant ataxin 3 bind beclin 1 more strongly than wild-type ataxin 3, but the mutant protein also has decreased deubiquitinase activity. This is likely to result in a partial dominant-negative effect of mutant ataxin 3 on beclin 1 levels, with similar consequences on this autophagy pathway as observed with mutant huntingtin fragments.

Apart from mutant huntingtin and ataxin 3, beclin 1 also interacted with atrophin 1 and the androgen receptor (Extended Data Fig. 10a, b), which are mutated in the polyQ diseases dentatorubral-pallidoluysian atrophy (DRPLA) and spinal and bulbar muscular atrophy, respectively. PolyQ-expanded atrophin 1 and androgen receptor showed increased interactions with beclin 1 that elevated beclin 1 K48-polyubiquitination (Extended Data Fig. 10a, b). Finally, we observed decreased beclin 1 levels and impaired starvation-induced autophagy in fibroblasts derived from patients with DRPLA, SCA3 or Huntington's disease, compared to controls (Fig. 4e–g, Extended Data Fig. 10c–g).

Our data reveal previously undescribed roles for polyQ tracts in health and disease. The wild-type ataxin 3 polyQ stretch is required for binding to beclin 1; binding enables deubiquitination of this key

autophagy inducer[26] and protects it from proteasome-mediated degradation. Importantly, this wild-type polyQ-mediated interaction was competed for by diverse disease-associated proteins with polyQ expansion mutations. The observed defect in starvation-induced autophagy caused by mutant polyQ proteins may reflect a less obvious impairment of basal autophagy, which is magnified under starvation conditions. This deficit may contribute to late-onset polyQ diseases, in which a relatively subtle defect is tolerated for decades before disease onset, and in which the toxic mutant protein itself is an autophagy substrate.

Online Content Methods, along with any additional Extended Data display items and Source Data, are available in the online version of the paper; references unique to these sections appear only in the online paper.

Received 10 November 2016; accepted 21 March 2017.
Published online 26 April 2017.

1. DiFiglia, M. *et al.* Aggregation of huntingtin in neuronal intranuclear inclusions and dystrophic neurites in brain. *Science* **277,** 1990–1993 (1997).
2. Riess, O., Rüb, U., Pastore, A., Bauer, P. & Schöls, L. SCA3: neurological features, pathogenesis and animal models. *Cerebellum* **7,** 125–137 (2008).
3. Imarisio, S. *et al.* Huntington's disease: from pathology and genetics to potential therapies. *Biochem. J.* **412,** 191–209 (2008).
4. Sathasivam, K. *et al.* Aberrant splicing of HTT generates the pathogenic exon 1 protein in Huntington disease. *Proc. Natl Acad. Sci. USA* **110,** 2366–2370 (2013).
5. Rubinsztein, D. C. The roles of intracellular protein-degradation pathways in neurodegeneration. *Nature* **443,** 780–786 (2006).
6. Arrasate, M., Mitra, S., Schweitzer, E. S., Segal, M. R. & Finkbeiner, S. Inclusion body formation reduces levels of mutant huntingtin and the risk of neuronal death. *Nature* **431,** 805–810 (2004).
7. Chai, Y., Berke, S. S., Cohen, R. E. & Paulson, H. L. Poly-ubiquitin binding by the polyglutamine disease protein ataxin-3 links its normal function to protein surveillance pathways. *J. Biol. Chem.* **279,** 3605–3611 (2004).
8. Burnett, B., Li, F. & Pittman, R. N. The polyglutamine neurodegenerative protein ataxin-3 binds polyubiquitylated proteins and has ubiquitin protease activity. *Hum. Mol. Genet.* **12,** 3195–3205 (2003).
9. Paulson, H. L. *et al.* Machado–Joseph disease gene product is a cytoplasmic protein widely expressed in brain. *Ann. Neurol.* **41,** 453–462 (1997).
10. Trottier, Y. *et al.* Heterogeneous intracellular localization and expression of ataxin-3. *Neurobiol. Dis.* **5,** 335–347 (1998).
11. Liang, X. H. *et al.* Induction of autophagy and inhibition of tumorigenesis by beclin 1. *Nature* **402,** 672–676 (1999).
12. Ravikumar, B. *et al.* Inhibition of mTOR induces autophagy and reduces toxicity of polyglutamine expansions in fly and mouse models of Huntington disease. *Nat. Genet.* **36,** 585–595 (2004).
13. Menzies, F. M. *et al.* Autophagy induction reduces mutant ataxin-3 levels and toxicity in a mouse model of spinocerebellar ataxia type 3. *Brain* **133,** 93–104 (2010).
14. Kabeya, Y. *et al.* LC3, a mammalian homologue of yeast Apg8p, is localized in autophagosome membranes after processing. *EMBO J.* **19,** 5720–5728 (2000).
15. Xie, Z. & Klionsky, D. J. Autophagosome formation: core machinery and adaptations. *Nat. Cell Biol.* **9,** 1102–1109 (2007).
16. Weidberg, H., Shvets, E. & Elazar, Z. Biogenesis and cargo selectivity of autophagosomes. *Annu. Rev. Biochem.* **80,** 125–156 (2011).
17. Tassa, A., Roux, M. P., Attaix, D. & Bechet, D. M. Class III phosphoinositide 3-kinase--Beclin1 complex mediates the amino acid-dependent regulation of autophagy in C2C12 myotubes. *Biochem. J.* **376,** 577–586 (2003).
18. He, R., Peng, J., Yuan, P., Xu, F. & Wei, W. Divergent roles of BECN1 in LC3 lipidation and autophagosomal function. *Autophagy* **11,** 740–747 (2015).
19. Dooley, H. C. *et al.* WIPI2 links LC3 conjugation with PI3P, autophagosome formation, and pathogen clearance by recruiting Atg12-5-16L1. *Mol. Cell* **55,** 238–252 (2014).
20. Vicinanza, M. *et al.* PI(5)P regulates autophagosome biogenesis. *Mol. Cell* **57,** 219–234 (2015).
21. Kim, W. *et al.* Systematic and quantitative assessment of the ubiquitin-modified proteome. *Mol. Cell* **44,** 325–340 (2011).
22. Rui, Y. N. *et al.* Huntingtin functions as a scaffold for selective macroautophagy. *Nat. Cell Biol.* **17,** 262–275 (2015).
23. Shibata, M. *et al.* Regulation of intracellular accumulation of mutant huntingtin by beclin 1. *J. Biol. Chem.* **281,** 14474–14485 (2006).
24. Trettel, F. *et al.* Dominant phenotypes produced by the HD mutation in STHdh(Q111) striatal cells. *Hum. Mol. Genet.* **9,** 2799–2809 (2000).
25. Nascimento-Ferreira, I. *et al.* Overexpression of the autophagic beclin-1 protein clears mutant ataxin-3 and alleviates Machado–Joseph disease. *Brain* **134,** 1400–1415 (2011).
26. Levine, B., Liu, R., Dong, X. & Zhong, Q. Beclin orthologs: integrative hubs of cell signaling, membrane trafficking, and physiology. *Trends Cell Biol.* **25,** 533–544 (2015).

Supplementary Information is available in the online version of the paper.

Acknowledgements We thank the Wellcome Trust (Principal Research Fellowship to D.C.R. (095317/Z/11/Z), Wellcome Trust Strategic Grant to Cambridge Institute for Medical Research (100140/Z/12/Z)), National Institute for Health Research Biomedical Research Centre at Addenbrooke's Hospital, and Addenbrooke's Charitable Trust and Federation of European Biochemical Societies (FEBS Long-Term Fellowship to A.A.) for funding; R. Antrobus for mass spectrometry analysis; S. Luo for truncated HTT constructs; M. Jimenez-Sanchez and C. Karabiyik for assistance with the primary mouse cell cultures; and J. Lim and Z. Ignatova for reagents.

Author Contributions A.A., C.F.B. and D.C.R. developed the study rationale. A.A. and D.C.R. wrote the manuscript, which was commented on by all authors. A.A. designed and performed most of the experiments. C.F.B. analysed some patient cell lines and structural models. T.R. and F.Si. performed mouse experiments. M.V. and M.C.H. performed and analysed confocal experiments. M.P. assisted with data analysis. S.I. contributed preliminary data. F.Sq. provided some control and patient samples. F.M.M. generated stable cell lines and constructs. D.C.R. supervised the study.

Author Information Reprints and permissions information is available at www.nature.com/reprints. The authors declare competing financial interests: details are available in the online version of the paper. Readers are welcome to comment on the online version of the paper. Publisher's note: Springer Nature remains neutral with regard to jurisdictional claims in published maps and institutional affiliations. Correspondence and requests for materials should be addressed to D.C.R. (dcr1000@cam.ac.uk).

Reviewer Information *Nature* thanks I. Dikic, J. Yuan and the other anonymous reviewer(s) for their contribution to the peer review of this work.

METHODS

Reagents. The primary antibodies used in the study include rabbit anti-actin (A2066), mouse anti-Flag M2 (F3165) and mouse anti-tubulin (T9026) from Sigma; rabbit anti-LC3 (NB 100-2220) and rabbit anti-atrophin-1 (NB100-2336) from Novus Biologicals; mouse anti-HA.11 (MMS-101P) from Covance; mouse anti-p62 (610833) from BD Bioscience; rabbit anti-beclin 1 (3738), rabbit anti-VPS34 (4263), rabbit anti-K48 polyUb (8081) and rabbit anti-K63 polyUb (5621) from Cell Signalling; rabbit anti-GFP (ab6556) from Abcam; mouse anti-ataxin 3 (MAB5360) and mouse anti-polyglutamine (MAB1574) from Millipore; mouse anti-GFP (632375) from Clontech; mouse anti-androgen receptor (sc-7305) from Santa Cruz; anti-mouse (NA931V) and anti-rabbit (NA934V) horseradish peroxidise (HRP)-conjugated secondary antibodies from GE Healthcare; goat anti-rabbit 800CW secondary antibodies (926-32211) from LI-COR; and Alexa Fluor 555- (A21428) conjugated goat anti-rabbit secondary antibodies from Invitrogen/Life Technologies. The constructs that were used in this work consisted of: empty pEGFP, HA–Ub, pEGFP-Q35 and pEGFP-Q81 as described in ref. 27. The following were a gift from H. Paulson[28]: pEGFP–ataxin 3Q28 (Addgene 22122), pEGFP–ataxin 3Q84 (22123), pFlag-6a–ataxin 3Q22 (Addgene 22126), pFlag-6a–ataxin 3Q22-C14A (Addgene 22127) and pFlag-6a–ataxin 3Q80 (Addgene 22129). The pcDNA4–Flag–beclin 1(1–242) (Addgene 24391) and pcDNA4–Flag–beclin 1(243–450) (Addgene 24392) constructs were gifts from Q. Zhong[29]. The following constructs were generated in our laboratory: pcDNA–Flag–beclin 1 and pcDNA–beclin 1 (ref. 30), pcDNA–Flag–beclin 1(K402R), pEGFP–ataxin 3 ΔQ(1–290), Flag–HTT 350 (1–350)[31], pEGFP–HTT exon 1 Q74 and pEGFP–HTT exon 1 Q23 (ref. 32) and Flag–full length HTT Q138. The following constructs were provided by J. Lim (HA-tagged androgen receptor with 25Q or 120Q) and Z. Ignatova (EGFP-tagged atrophin-1 with 19Q or 71Q).

Cell lines. Human cervical carcinoma (HeLa) cells and striatal neuronal cell lines derived from wild-type HTT Q7/Q7 and heterozygous HTT Q7/Q111 knock-in mice (Coriell Institute CH00097 and CH00096, respectively) were grown at 37 °C (for HeLa) and at 33 °C (for striatal cells) in DMEM (Sigma) supplemented with 10% FBS, 100 U ml^{-1} penicillin/streptomycin, 2 mM L-glutamine and 1 mM sodium pyruvate (basal medium) in 5% CO_2. HeLa cells stably expressing GFP–LC3 and HeLa cells stably expressing the mTagRFP–mWasabi–LC3 reporter were cultured in basal medium supplemented with 500 μg ml^{-1} G418 (Sigma). For creation of mTagRFP–mWasabi–LC3 stable cell lines, mTagRFP–mWasabi–LC3 (construct from J. Lin[33]) was cloned into pIRESneo using EcoR1 and SacII sites. The construct was transfected into HeLa cells, and transfected cells were selected using G418. Single-cell clones were generated by fluorescence-activated cell sorting (FACS) and cell lines showing moderate expression were selected. mTagRFP–mWasabi–LC3 monitors autophagic flux, as mWasabi (green) fluorescence is quenched when autophagosomes are acidified following fusion with lysosomes. Stable inducible HEK293 cells expressing wild-type (Q23) or mutant (Q74) huntingtin (HTT) exon 1 were generated by cloning GFP–HTT (mutant or wild-type) from eGFP–C1 into pCDNA5/TO using Xba1 and ApaI restriction sites. These constructs were linearized with MfeI and transfected into T-Rex-293 cells (Thermo Fisher), which stably express the tetracycline repressor protein. Transfected cells were selected by addition of hygromycin. Single-cell clones were generated, which showed expression of GFP–HTT only in the presence of doxycycline, and to enable comparison, with similar levels of HTT expression. HeLa cells (source ATCC) and HEK293 cells (source ECACC) were authenticated by STR profiling and were routinely tested for mycoplasma contamination. In some experiments, cells were starved in Hanks balanced salt solution (HBSS) medium (Invitrogen) for 4 h with or without 400 nM of bafilomycin A1 (BafA1) (Sigma). BafA1 treatment alone was carried out sometimes for 16 h with 200 nM, as indicated in the legends. Cell transfection was performed with TransIT 2020 Mirus (for DNA) or Lipofectamine 2000 reagents (for siRNA) (Invitrogen), using the manufacturers' protocols. Final siRNA concentrations of 20–100 nM were used for silencing with two rounds of knockdown for 5 days. The following oligonucleotides (ON-TARGETplus SMARTpool, Dharmacon) were used for ataxin 3 depletion: oligo 05 (ACAGGAAGGUUAUUCUAUA), oligo 06 (a) (GGACAGAGUUCACAUCCAU), oligo 07 (b) (GCACUAAGUCGCCAAGAAA), oligo 08 (GCAGGGCUAUUCAGCUAAG); for beclin 1 depletion: oligo 05 (GAUACCGACUUGUUCCUUA), oligo 06 (GGAACUCACAGCUCCAUUA), oligo 07 (CUAAGGAGCUGCCGUUAUA), oligo 08 (GAGAGGAGCCAUUUAUUGA).

Ataxin 3 depletion in mice. All studies and procedures were performed with project licences granted by the UK Home Office and with the approval of the University of Cambridge Committee for Animal Studies. C57BL/6J mice (Jackson Laboratories) were depleted of ataxin 3 in the liver using the ThermoFisher Invivofectamine 3.0 system. The siRNA duplex solution was prepared and diluted to 2.4 mg ml^{-1} according to the manufacturer's instructions. Preparation of the final injection solution was also in accordance with the Thermofisher protocol. Briefly, siRNA (control/scrambled siRNA 4457289; ataxin 3 siRNA 4457308) was mixed with the complexation buffer and then the Invivofectamine 3.0 reagent (IVF3005, ThermoFisher). The ataxin 3 siRNA was an Ambion pre-designed sequence: sense (5–3): GCAUCGACCAAAACUUAUUtt; antisense (5–3): AAUAAGUUUUGGUCGAUGCat. The solution was vortexed, incubated at 50 °C for 30 min and then diluted in PBS. The solution was stored at 4 °C and later up to 200 μl was injected into the lateral caudal vein at a final concentration of 1 mg kg^{-1}. Mice were monitored for any adverse side effects briefly after injection with none observed. Mice used were female, weighing approximately 20 g at the age of 6 weeks. Mice were randomly selected for injection with control or targeting siRNA and were matched by weight. The knockdown was left for 5 days. On the fourth day, the mice were deprived of food for a total period of 24 h with free access to water throughout the procedure. Livers from these mice were dissected, homogenized and resuspended in tissue lysis buffer on ice (50 mM Tris pH 7.4, 0.5% Triton X-100 and protease inhibitor cocktail) and the supernatant was centrifuged twice. Proteins were resolved by SDS–PAGE for further analysis. The same control was loaded onto each gel and the samples were normalized to that same control on the same gel to allow comparison between multiple samples. The animal experiments did not involve behavioural testing but focused on biochemistry; therefore, the samples were not blinded at this stage as we wanted to be able to load the gels in a suitable order.

Food deprivation in Huntington's disease model mice. We used HD-N171-82Q mice (B6C3F1/J-Tg(HD82Gln)81 Dbo/J, Jackson Laboratory). These mice carry an N-terminal fragment expressing the first 171 amino acids of human huntingtin with 82 glutamine repeats under the mouse prion promotor[34]. The Huntington's disease transgenic mice and non-transgenic littermates were males and females at the age of 6 weeks in the study. The mice fasted and were deprived of food for a total period of 48 h with free access to water throughout the procedure. After 22.5 h starvation, mice were given free access to food for 1.5 h followed by a second round of starvation for another 22.5 h. At the end of this period, the mice were killed by a schedule 1 method. The brain was collected and frozen for western blot analysis. The mice were weighed at every stage of this experiment in order to monitor weight loss. Half brain samples from starved and fed mice were dissected, homogenized and resuspended in tissue lysis buffer on ice (50 mM Tris pH 7.4, 0.5% Triton X-100 and protease inhibitor cocktail) and the supernatant was centrifuged twice. Proteins were resolved by SDS–PAGE for further analysis.

Immunohistochemistry. Thirty-micrometre sections of brains derived from Huntington's disease transgenic young and adult mice (6 and 12 weeks old, respectively) were analysed for neuronal aggregates as described[35]. Sections were labelled with anti-huntingtin antibody (clone mEM48, Chemicon, MAB5374) by free-floating immunohistochemistry. Staining was performed by peroxidase labelling using Vectastain Avidin:Biotinylated enzyme complex (ABC) kit and visualized with DAB reagent (Vector Laboratories). Aggregates were counted in the motor cortex in three fields on at least three sections per animal at a magnification of ×100 (Zeiss Axioskop2, field diameter 0.2 mm) and analysed for the average of aggregates in brains from young and adult Huntington's disease transgenic mice. The observer was blinded to the identity of the samples.

Analysis of patient cells. Primary fibroblasts from 9 controls and 13 patients with mutant polyQ diseases were grown at 37 °C in DMEM supplemented with 10% FBS, 100 U ml^{-1} penicillin/streptomycin, GlutaMAX 1:100 (35050061, ThermoFisher) and 1 mM sodium pyruvate (basal medium) under 5% CO_2. In some experiments, cells were starved in HBSS medium for 4 h or treated for 4 h with 400 nM BafA1. The following patient fibroblasts were obtained from Coriell Biorepository, Coriell Institute for Medical Research: Huntington's disease (HD) (GM04285, GM04287, GM04476, GM04867), DRPLA (GM13716, GM13717), SCA3 (GM06151, GM06153) and SCA7 (GM03561). The following patient fibroblasts were provided by F.Sq. A program to collect biological specimens at the Mendel Institute of Human Genetics for research purposes, including skin biopsies to derive fibroblast cell lines, was approved by the Ethical Committee from Casa Sollievo della Sofferenza Foundation, section of Istituto Tumori Giovanni Paolo II in Bari. Informed consent was obtained from healthy control subjects and from patients with DRPLA (AT2140102) or Huntington's disease (HD 940-01, HD960-01) and from the legal representative of another patient with Huntington's disease (HD305-01). See Supplementary Table 2 for a list of patient fibroblasts, their catalogue numbers and the matching reference numbers in the paper.

Isolation and culture of primary cortical neurons. Primary cortical neurons were isolated from C57BL/6 mouse (Jackson Laboratories) embryos at embryonic day (E)16.5 as previously described[32]. Briefly, embryo brains were harvested and placed in PBS/glucose where the meninges were removed and the cerebral cortices were dissected. After mechanical dissociation using sterile micropipette tips, dissociated neurons were resuspended in PBS/glucose and collected by centrifugation. Viable

cells were seeded on poly-ornithine-coated 12-multiwell plates. Cells were cultured in neurobasal medium supplemented with 2 mM glutamine, 200 mM B27 supplement and 1% penicillin/streptomycin at 37 °C in a humidified incubator with 5% CO_2. One half of the culture medium was changed every two days until treatment or infection. After 5 days of *ex vivo* culturing, differentiated neurons were infected with lentiviral particles.

Lentivirus production and infection. Short hairpin RNA lentiviral particles were produced and transduced following The RNAi Consortium (TRC) protocols. shRNA containing pLKO.1 vectors targeting mouse *Atxn3* were obtained from The RNAi Consortium (TRCN0000123959 and TRCN0000123961). Scramble shRNA was a gift from D. Sabatini (Addgene plasmid 1864)[36]. Briefly, HEK293T packaging cells growing in 10-cm dishes were transfected with a mix of 2.5 μg packaging vector (psPAX2), 270 ng envelope vector (pMD2.G) and 2.7 μg hairpin-pLKO.1 vector. TransIT-LT1 (Mirus) was used as transfection reagent. After transfection, cells were cultured in high-serum medium. Cell culture medium was collected 40 h later and replaced by high-serum medium; this step was repeated 2–3 times at intervals of 24 h. Virus preparations were then concentrated by centrifugation at 30,000 r.p.m. for 90 min. Viral particles were added to primary cultured neurons and incubated overnight. After 24 h, medium was replaced by full medium and cells were incubated for 5 more days. For autophagy flux experiments, neurons were treated with 200 nM BafA1 in full medium for 16 h or starved in HBSS with 400 nM BafA1 for 4 h.

Western blot analysis. Cells were lysed in lysis buffer (20 mM Tris-HCl, pH 6.8, 137 mM NaCl, 1 mM EGTA, 1% Triton X-100, 10% glycerol and protease inhibitors cocktail) and protein samples were boiled in Laemmli buffer for 5–7 min at 100 °C, separated by SDS–PAGE, transferred onto PVDF membranes, subjected to western blot analysis, and visualized using an ECL enhanced chemiluminescence detection kit (GE Healthcare), or with direct infrared fluorescence detection on an Odyssey Infrared Imaging System.

Immunoprecipitation and ubiquitination assays. Cells were lysed with IP buffer (20 mM Tris-HCl, pH 7.2, 150 mM NaCl, 2 mM $MgCl_2$, 0.5% NP-40 and protease inhibitors cocktail). For ubiquitination experiments, cells were treated with a proteasome inhibitor MG132 (10 μM) in the last 6 h before lysis with the IP buffer supplemented with 1 mM PMSF and 10 mM iodoacetamide. Whole-cell lysates obtained by centrifugation were incubated with 2–5 μg of antibody overnight at 4 °C followed by 2 h incubation with protein A sepharose beads (GE Healthcare). The immunocomplexes were then washed with IP buffer for three times and separated by SDS–PAGE for further western blotting assay.

***In-vitro* deubiquitination assay.** Ubiquitinated beclin 1 was purified from HeLa cells transfected with expression vectors for HA–Ub and Flag–beclin 1 for 24 h as previously described[37]. For the last 6 h, the cells were treated with a proteasome inhibitor MG132 (10 μM) and a 10 μM cell-permeable, non-selective DUB inhibitor PR616 (ab144641, Abcam). Ubiquitinated beclin 1 was purified from cell lysates with anti-Flag-affinity beads (Sigma, A2220) in Flag lysis buffer (20 mM Tris-HCl, pH 6.8, 137 mM NaCl, 1 mM EGTA, 1% Triton X-100, 1 mM DTT, 10% glycerol and protease inhibitors cocktail). After washing with the Flag-lysis buffer, the proteins were eluted with 3× Flag peptides (F4799, Sigma). Recombinant ataxin-3 Q22 and Flag–ataxin 3 Q22 C14A were expressed in HeLa cells and purified using Flag affinity beads and eluted with 3× Flag peptides. In the *in vitro* deubiquitination assay, ubiquitinated beclin 1 was incubated with recombinant ataxin 3 in the deubiquitination buffer (50 mM Tris-HCl (pH 8.8), 50 mM NaCl, 5% glycerol, 10 mM DTT, 1 mM EDTA) at 37 °C.

Fluorescence microscopy. The cells were grown on coverslips and were fixed in 4% paraformaldehyde (for LC3–GFP) or methanol (for endogenous LC3, 1:150 Novus Biologicals) for 5 min and then permeabilized with 0.1% Triton X-100. For blocking and primary and secondary antibodies, 1% BSA in PBS was used. The staining of PtdIns3P was performed as described in ref. 38. Briefly, cells were fixed in 2% paraformaldehyde and permeabilized with 20 μM digitonin in buffer A (20 mM Pipes pH 6.8, 137 mM NaCl, 2.7 mM KCl). Then cells were blocked with buffer A supplemented with 5% (v/v) FBS and 50 mM NH_4Cl. Anti- PtdIns3P antibodies from Echelon (for 1 h, 1:300) and secondary antibodies were applied in buffer A with 5% FBS. Cells were post-fixed for 5 min in 2% paraformaldehyde, washed with PBS containing 50 mM NH_4Cl, washed once with water and then mounted with Mowiol. For WIPI2 staining, cells were grown on coverslips at 60% confluency and were incubated in EBSS for 1 h. Then cells in 1 ml EBSS were fixed by the addition of 1 ml 4% paraformaldehyde to a final concentration of 2% and incubated for 10 min at room temperature and then cells were permeabilized with 0.1% Triton X-100. 1% BSA PBS solution was used for blocking before adding primary antibody (mouse anti-WIPI2, 1:100 Abcam ab105459). A Zeiss LSM880 confocal microscope was used for fluorescent confocal analysis. All confocal images were taken with a 63× oil-immersion lens. Microscopy assays (for example, dot quantification) were performed by selecting fields based on nuclear and GFP staining (with the channel for the dots turned off)—thus the operator was blinded to the outcome of the experiment when selecting suitably similar fields to image for subsequent computerised analysis. ImageJ was used for the analysis (number of vesicles or puncta). For the analysis of WIPI2 puncta that involved different cell lines in different conditions, we used a custom-designed image-processing pipeline in ImageJ. First, an estimation of the cytoplasmic area was made by simultaneously expanding an area from each nuclear centroid, until a neighbouring expansion is detected. The resulting mask represents individual cells and was subsequently used to identify WIPI2 dots. Identification of the dots started by reducing cytoplasmic background signal through application of a Gaussian convolution filter. The resulting image was then binarized according to the Chow and Kaneko adaptive thresholding method. Subsequently, connected or clustered dots were separated using a classic watershed segmentation algorithm. Consecutive quantification and feature extraction were then performed on all dots that met set size parameters. Automated microscope counting of autolysosomes labelled with a pH-sensitive mTagRFP–mWasabi–LC3 was carried out using a Thermo Scientific Cellomics ArrayScan VTI HCS reader and the Spot Detector Bioapplication protocol, as described[20]. About 800 cells per condition were analysed.

Addition of exogenous PtdIns3P to cells. PtdIns3P di-C16 and carrier (Echelon) were reconstituted in H_2O:tert-BuOH (9:1) solution. After 1 min bath sonication, carrier and PtdIns3P di-C16 were combined at a 1:1 ratio for 10 min at room temperature. The mixture of PtdIns3P di-C16 and carrier were diluted in medium and used for 1–2 h incubations of cells. The final concentration used was 1 μM. For the negative control, DMEM was combined with carrier only and added to the cells.

Mass spectrometry. HeLa cells were transfected with Flag–beclin 1 and HA–Ub for 24 h and treated for the last 6 h with proteasome inhibitor (MG132 10 μM), and Flag beclin 1 was immunoprecipitated for identification of putative sites of ubiquitination using mass spectrometry. Samples were resolved into a pre-cast 4–12% Bis-Tris polyacrylamide gel (Novex, Thermo Fisher Scientific). The lanes were excised and cut into three approximately equal chunks and the proteins reduced, alkylated and digested in-gel. The resulting tryptic peptides were analysed by LC-MSMS using a Q Exactive coupled to an RSLCnano3000 (Thermo Scientific). Raw files were processed in Proteome Discoverer 1.4 using Sequest to search a human Uniprot database (downloaded 03/06/14, 20,176 entries). GlyGly (K) was set as a variable modification and carbamidomethyl (C) as a fixed modification. Peptides were filtered to high confidence (0.01 false discovery rate, FDR) using Percolator.

Structural analysis of polyQ binding to beclin 1. Glide software (Schrödinger, LLC) was used for studying potential ligand (polyQ7 stretch)–receptor (human beclin 1 ECD; pdb 4DDP, ref. 39) interactions. Protein and ligand preparation were performed first, followed by generation of possible ligand binding sites using site-map. A receptor grid was then generated for each of the putative binding sites and standard precision peptide (SP-peptide) docking was performed. Although several potential binding sites were found, docking scores for two of the sites were substantially higher than for the others. It should be noted that that binding sites surrounding the N-terminal helix of beclin 1 ECD (pdb 4DDP) were not considered, as the yeast Vps30-BARA domain structure (pdb 5DFZ, ref. 40) shows that this helix is likely to be out of place, being part of the coiled-coil domain (CCD) of beclin 1. Docking poses from the best sites were used to generate figures. Visualization and generation of graphic illustrations of the molecular models were performed using PyMOL (http://www.pymol.org).

Statistics. Statistical analysis was done using Microsoft Excel and GraphPad Prism v5. For ANOVA analysis involving multiple sample comparisons, post testing was performed to discriminate significance relationships. For *t*-test analysis, one-tailed test were performed for independent samples, as indicated in the figure legends. Error bars shown in the figures are standard deviation (s.d.) or standard error (s.e.m.), as stated. Sample sizes were chosen on the basis of extensive experience with the assays we have performed. The experiments were appropriately randomized.

Data availability. Gel source images are provided in Supplementary Fig. 1. Other source data and reagents can be provided by the authors upon reasonable request. Beclin 1 structures were from Protein Data Bank (pdb 4DDP, pdb 5DFZ). Beclin 1 protein sequences were from UniProt (human Q14457, mouse O88597, zebrafish A2A135).

27. Onodera, O. *et al.* Oligomerization of expanded-polyglutamine domain fluorescent fusion proteins in cultured mammalian cells. *Biochem. Biophys. Res. Commun.* **238,** 599–605 (1997).
28. Chai, Y., Shao, J., Miller, V. M., Williams, A. & Paulson, H. L. Live-cell imaging reveals divergent intracellular dynamics of polyglutamine disease proteins and supports a sequestration model of pathogenesis. *Proc. Natl Acad. Sci. USA* **99,** 9310–9315 (2002).

29. Sun, Q. *et al.* Identification of Barkor as a mammalian autophagy-specific factor for Beclin 1 and class III phosphatidylinositol 3-kinase. *Proc. Natl Acad. Sci. USA* **105,** 19211–19216 (2008).
30. Luo, S. *et al.* Bim inhibits autophagy by recruiting Beclin 1 to microtubules. *Mol. Cell* **47,** 359–370 (2012).
31. Eriguchi, M. *et al.* alpha Pix enhances mutant huntingtin aggregation. *J. Neurol. Sci.* **290,** 80–85 (2010).
32. Jimenez-Sanchez, M. *et al.* siRNA screen identifies QPCT as a druggable target for Huntington's disease. *Nat. Chem. Biol.* **11,** 347–354 (2015).
33. Zhou, C. *et al.* Monitoring autophagic flux by an improved tandem fluorescent-tagged LC3 (mTagRFP-mWasabi-LC3) reveals that high-dose rapamycin impairs autophagic flux in cancer cells. *Autophagy* **8,** 1215–1226 (2012).
34. Schilling, G. *et al.* Intranuclear inclusions and neuritic aggregates in transgenic mice expressing a mutant N-terminal fragment of huntingtin. *Hum. Mol. Genet.* **8,** 397–407 (1999).
35. Davies, S. W. *et al.* Detection of polyglutamine aggregation in mouse models. *Methods Enzymol.* **309,** 687–701 (1999).
36. Sarbassov, D. D., Guertin, D. A., Ali, S. M. & Sabatini, D. M. Phosphorylation and regulation of Akt/PKB by the rictor–mTOR complex. *Science* **307,** 1098–1101 (2005).
37. Liu, J. *et al.* Beclin1 controls the levels of p53 by regulating the deubiquitination activity of USP10 and USP13. *Cell* **147,** 223–234 (2011).
38. Hammond, G. R., Schiavo, G. & Irvine, R. F. Immunocytochemical techniques reveal multiple, distinct cellular pools of PtdIns4P and PtdIns(4,5)P(2). *Biochem. J.* **422,** 23–35 (2009).
39. Huang, W. *et al.* Crystal structure and biochemical analyses reveal Beclin 1 as a novel membrane binding protein. *Cell Res.* **22,** 473–489 (2012).
40. Rostislavleva, K. *et al.* Structure and flexibility of the endosomal Vps34 complex reveals the basis of its function on membranes. *Science* **350,** aac7365 (2015).

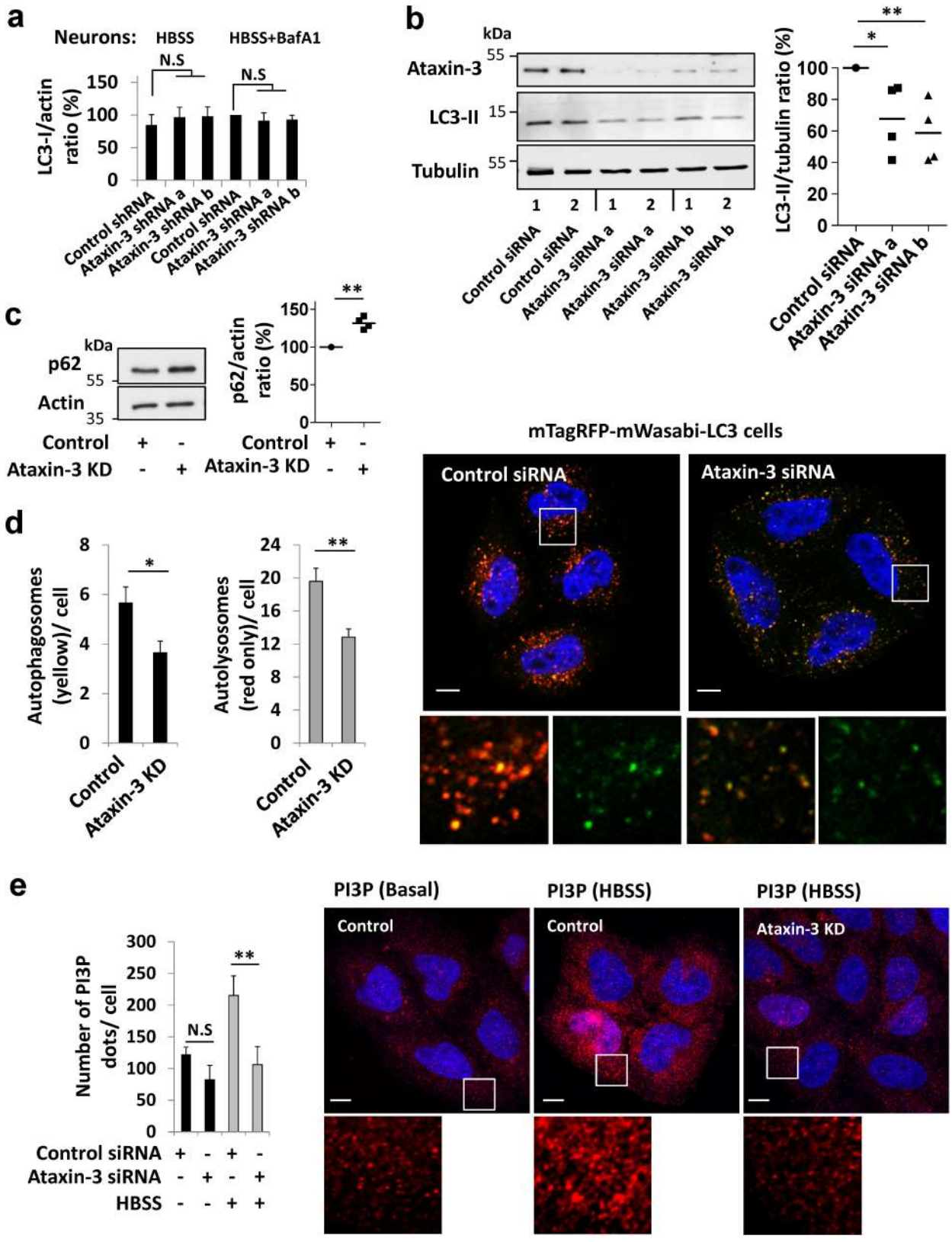

Extended Data Figure 1 | See next page for caption.

Extended Data Figure 1 | Ataxin 3 contributes to autophagosome formation. a, Primary cultures of mouse cortical neurons were transduced with control or *Atxn3* lentiviral shRNAs and analysed for the levels of LC3-I under starvation condition (HBSS, 4 h) or with BafA1 (400 nM, 4 h). Results are normalized to control cells (HBSS + BafA1). Mean ± s.e.m., $n = 5$ replicates from two independent cultures. Two-way ANOVA (NS, not significant). **b**, HeLa cells were transfected with different *Atxn3* siRNAs or scrambled siRNA as a control. Ataxin 3 knockdown (KD) efficiency is presented as well as basal LC3-II levels. LC3-II levels in ataxin-3-depleted HeLa cells were normalized to control cells; $n = 4$ independent experiments. One-way ANOVA with post hoc Tukey's test. **c**, p62 levels in HeLa cells depleted of ataxin 3 by siRNA. p62 levels were normalized to control cells ($n = 4$ independent experiments, one-tailed paired *t*-test). **d**, HeLa cells stably expressing mTagRFP–mWasabi–LC3 reporter were transfected with either scrambled or *Atxn3* siRNA and were analysed with the ThermoFisher cellomics system to assess the number of autophagosomes and autolysosomes in the cells. Results are mean number of autophagosomes or autolysosomes per cell ± s.e.m. in eight fields from a representative experiment out of three independent experiments (one-tailed unpaired *t*-test). Representative images of the cells were taken by confocal microscopy (total 800 cells). Scale bars, 10 μm. **e**, Control and ataxin 3 KD HeLa cells were starved (HBSS, 4 h) or kept in full medium. The number of PtdIns3P (PI3P) phospholipid dots was analysed by staining with anti-PtdIns3P antibody. Results are mean dots per cell ± s.d. from a representative experiment out of three independent experiments as well as representative confocal images of PtdIns3P dots (red) for each condition ($n = 20$ cells). Scale bars, 10 μm. Two-way ANOVA (column factor siRNA $P < 0.001$, row factor starvation $P < 0.01$, interaction $P < 0.05$) with Bonferroni's post-test. $^{*}P < 0.05$, $^{**}P < 0.01$, NS, not significant.

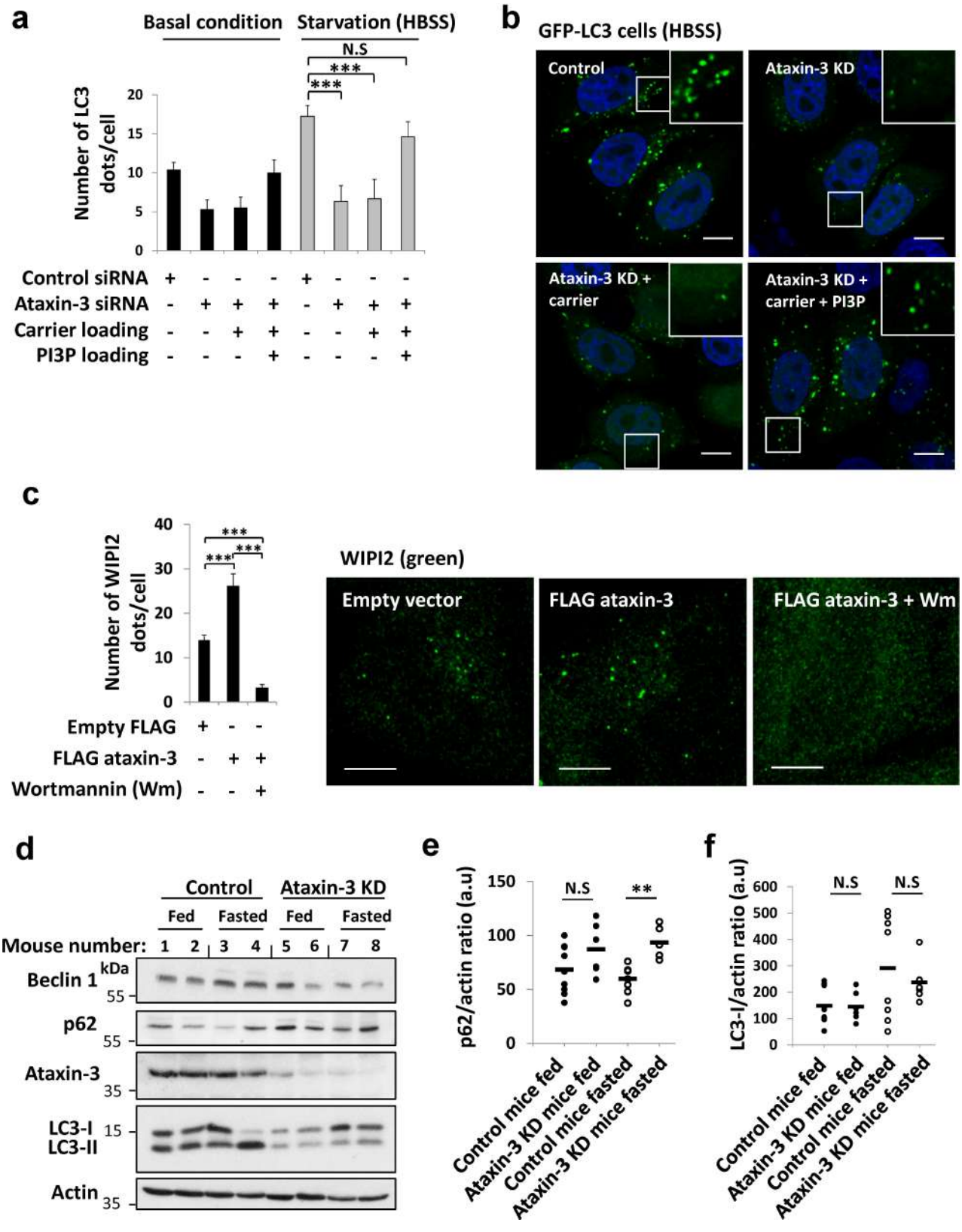

Extended Data Figure 2 | See next page for caption.

Extended Data Figure 2 | Ataxin 3 regulates starvation-induced autophagy. a, **b**, HeLa cells stably expressing GFP–LC3 were treated with control or *Atxn3* siRNA and incubated for 1 h with carrier alone or carrier with 1 μM PtdIns3P phospholipid. Then, the control cells and ataxin 3 KD cells with the different treatments were shifted to starvation conditions (HBSS, 4 h) or kept in full medium. **a**, The number of LC3 dots was analysed for each of the conditions and presented as mean LC3 dots per cell ± s.e.m, determined from $n = 5$ fields from a single representative experiment out of three independent experiments. Two-way ANOVA (column factor siRNA $P < 0.001$, row factor starvation $P < 0.05$, interaction P value not significant (NS)) with Bonferroni's post-test: for basal condition, NS; for starvation, $P < 0.001$. **b**, Representative confocal images of LC3 dots (green) from the different treatments are presented for the starvation condition. For **a** and **b**, the total number of cells analysed in basal control, $n = 25$; basal KD, basal KD carrier, basal KD carrier PtdIns3P, $n = 30$; HBSS control, $n = 34$; HBSS KD, HBSS KD carrier PtdIns3P, $n = 37$; HBSS KD carrier, $n = 32$. Scale bars, 10 μm. **c**, Number of dots of the endogenous PtdIns3P effector, WIPI2, in HeLa cells that were transfected with Flag–ataxin 3 or empty vector and starved (EBSS, 1 h) with or without the PtdIns3P inhibitor Wortmannin (Wm, 20 nM). Data are presented as means ± s.e.m. of the number of WIPI2 dots per cell determined from the total number of cells analysed using software described in Methods from a representative experiment out of two independent experiments. Confocal images of WIPI2 dots (green) from the different treatments are shown. Number of cells analysed and used for the s.e.m. in empty Flag, $n = 47$; Flag–ataxin 3, $n = 45$; Flag–ataxin 3/Wm, $n = 37$. Scale bars, 10 μm. One-way ANOVA with post hoc Tukey's test. **d**–**f**, Mice were depleted of ataxin 3 in the liver by injection of *Atxn3* siRNA or control/scrambled siRNA formulations into the lateral caudal vein. The knockdown was left for 5 days with fasting on the fourth day. Livers from these mice were dissected and homogenized and proteins were resolved by SDS–PAGE. **d**, Representative blots and *in vivo* ataxin 3 knockdown efficiency. For quantification of beclin 1 and LC3-II, see Fig. 1d, e. **e**, Quantification of p62 levels; **f**, quantification of LC3-I levels in each group of mice (control fed, $n = 9$; ataxin 3 KD fed, $n = 6$; control fasted, $n = 8$, ataxin 3 KD fasted, $n = 6$; a.u, arbitrary units). **e**, Two-way ANOVA (column factor siRNA $P < 0.05$, row factor fasting $P < 0.05$, interaction $P < 0.05$) with Bonferroni's post-test. For **f**, two-way ANOVA (column factor siRNA NS, row factor starvation $P < 0.05$, interaction NS) with Bonferroni's post-test (NS). This suggests no obvious difference in LC3-I levels between the control and ataxin-3 KD groups. $^{**}P < 0.01$, $^{***}P < 0.001$.

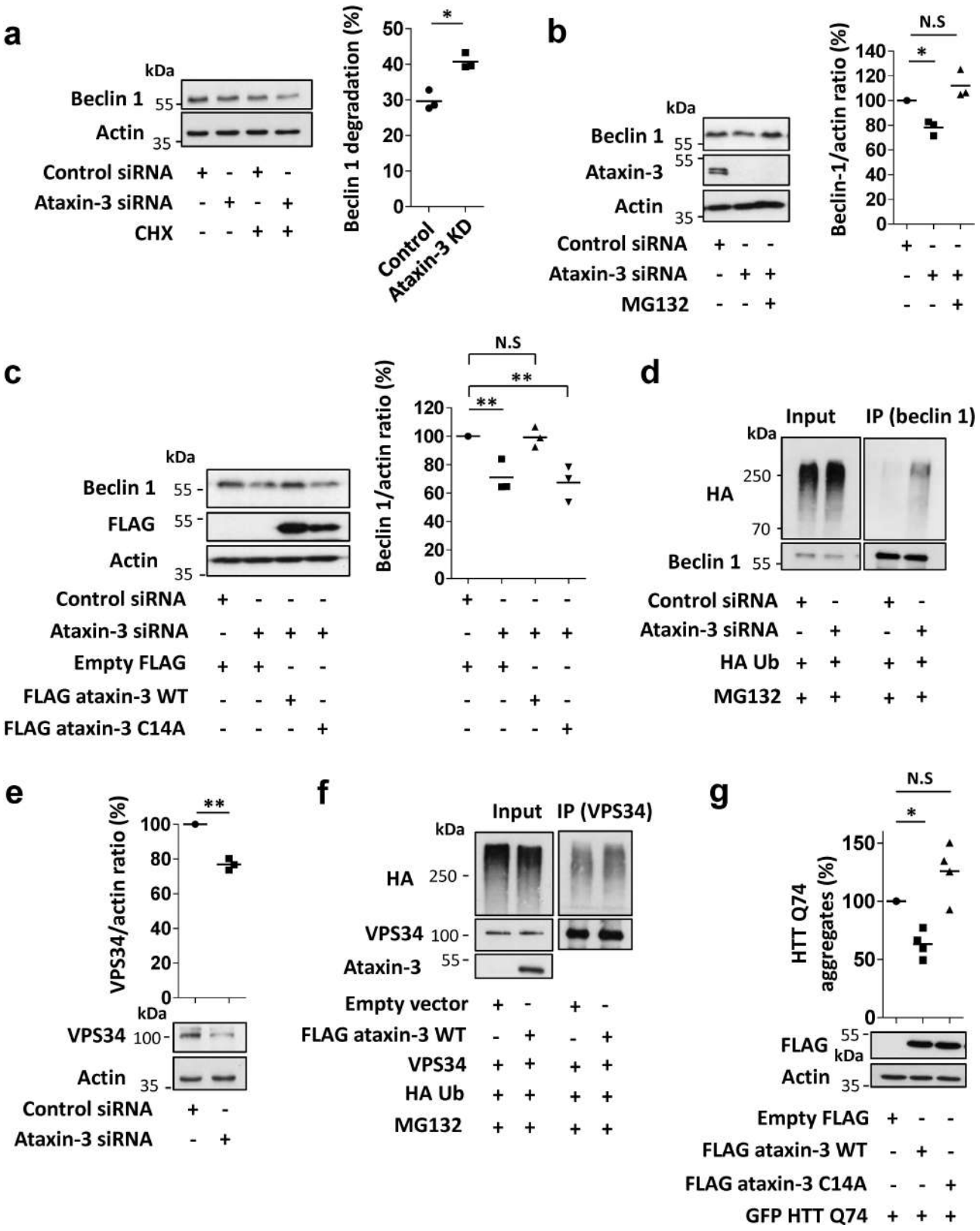

Extended Data Figure 3 | See next page for caption.

Extended Data Figure 3 | Ataxin 3 regulates beclin 1 stability and ubiquitination. a, Beclin 1 levels in control siRNA-treated HeLa cells and ataxin 3 KD cells ($t = 0$) and after cycloheximide (CHX, 50 μg ml^{-1}) treatment ($t = 8$ h). The percentage of beclin 1 degradation in control or ataxin 3 KD cells was determined by comparing to cells without CHX treatment ($n = 3$ independent experiments, one-tailed paired t-test). **b**, Beclin 1 levels in control siRNA-treated HeLa cells and ataxin 3 KD cells that were treated for the last 6 h with proteasome inhibitor (MG132, 5 μM). $n = 3$ independent experiments, one-way ANOVA ($P < 0.01$) with post hoc Tukey's test. **c**, Beclin 1 levels in ataxin-3-depleted HeLa cells that were transfected with wild-type (WT) Flag–ataxin 3 or protease-dead mutant FLAG–ataxin 3 C14A for 48 h. Results normalized to control siRNA, $n = 3$ independent experiments, one-way ANOVA ($P < 0.01$) with post hoc Tukey's test. **d**, Control siRNA-treated and *Atxn3* siRNA-treated HeLa cells were transfected with the indicated vectors for 24 h and treated for the last 6 h with MG132 (10 μM). Endogenous beclin 1 was immunoprecipitated to detect beclin 1 ubiquitination. **e**, VPS34 levels in ataxin-3-depleted HeLa cells normalized to control siRNA, $n = 3$ independent experiments. One-tailed paired t-test. **f**, HeLa cells were transfected with the indicated vectors for 24 h and treated for the last 6 h with MG132 (10 μM). VPS34 was immunoprecipitated to detect VPS34 ubiquitination. The levels of the VPS34 components are co-ordinately regulated, and decreased beclin 1 levels in ataxin-3-depleted cells were accompanied by decreased levels of VPS34. Still, no obvious change in VPS34 ubiquitination was observed in ataxin-3-overexpressing cells, supporting a selective effect on beclin 1. **g**, Flag–ataxin 3 WT and Flag–ataxin 3 C14A were co-expressed with GFP–huntingtin (HTT) exon 1 Q74 in HeLa cells for 48 h. The number of aggregates was analysed by monitoring GFP fluorescence in 400 cells. $n = 4$ independent experiments. Results normalized to control (empty vector). One-way ANOVA ($P < 0.01$) with post hoc Tukey's test. $^{*}P < 0.05$, $^{**}P < 0.01$, NS, not significant.

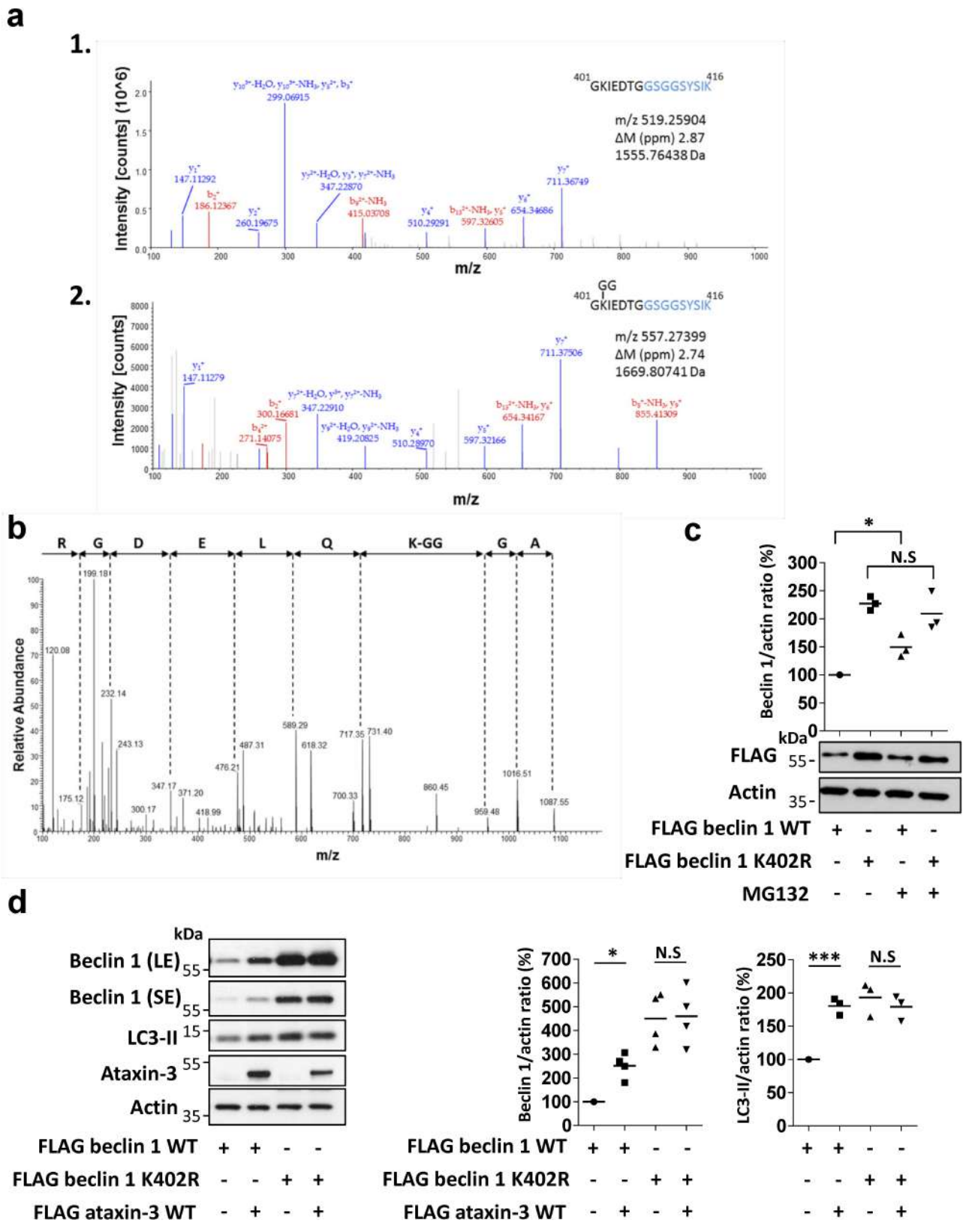

Extended Data Figure 4 | See next page for caption.

Extended Data Figure 4 | Analysis of beclin 1 lysine 402 modification. **a**, **b**, HeLa cells were transfected with Flag–beclin 1 and HA–Ub for 24 h and treated for the last 6 h with MG132 (10 μM). Flag–beclin 1 was immunoprecipitated for mass spectrometry analysis. Tryptic digests of ubiquitin-conjugated beclin 1 resulted in peptides that contain a ubiquitin remnant derived from the ubiquitin C terminus ('GG' motif). **a**, Identification of a putative site of ubiquitination in beclin 1. Top, MS–MS spectrum of the unmodified beclin 1 peptide spanning residues 401–416. Amino acids with corresponding y ions are shown in blue. Bottom, MS–MS spectrum of an ion with a mass 114 Da greater than the unmodified peptide. The matching y ions and presence of a modified b2 ion indicate –GG modification of lysine 402. **b**, MS–MS spectra filtered to high confidence covering 100% of the ubiquitin sequence. Tryptic peptide spanning residues 43–54 including lysine 48 was identified as the sole high-confidence peptide with a modification corresponding to a –GG motif and the MS–MS spectra of the peptide demonstrate fragments corresponding to a –GG modified lysine 48. **c**, Levels of Flag–beclin 1 and Flag–beclin 1 K402R in HeLa cells that were treated for the last 6 h with MG132 (10 μM). Results normalized to control (Flag–beclin 1 WT). $n = 3$ replicates from two independent experiments. Two-way ANOVA (column factor K402R NS, row factor MG132 $P < 0.001$, interaction $P < 0.05$) with Bonferroni's post-test. **d**, HeLa cells were transfected with the indicated vectors for 24 h and shifted in the last 4 h to HBSS. Beclin 1 and LC3-II levels were analysed and results normalized to control (Flag–beclin 1 WT). For LC3-II levels, $n = 3$ independent experiments, two-way ANOVA (column factor ataxin 3 $P < 0.05$, row factor K402R mutation $P < 0.01$, interaction $P < 0.01$) with Bonferroni's post-test. For beclin 1 levels, $n = 4$ independent experiments, two-way ANOVA (column factor ataxin 3 $P < 0.05$, row factor K402R mutation $P < 0.001$, interaction NS) with Bonferroni's post-test. $^{*}P < 0.05$, $^{***}P < 0.001$, NS, not significant.

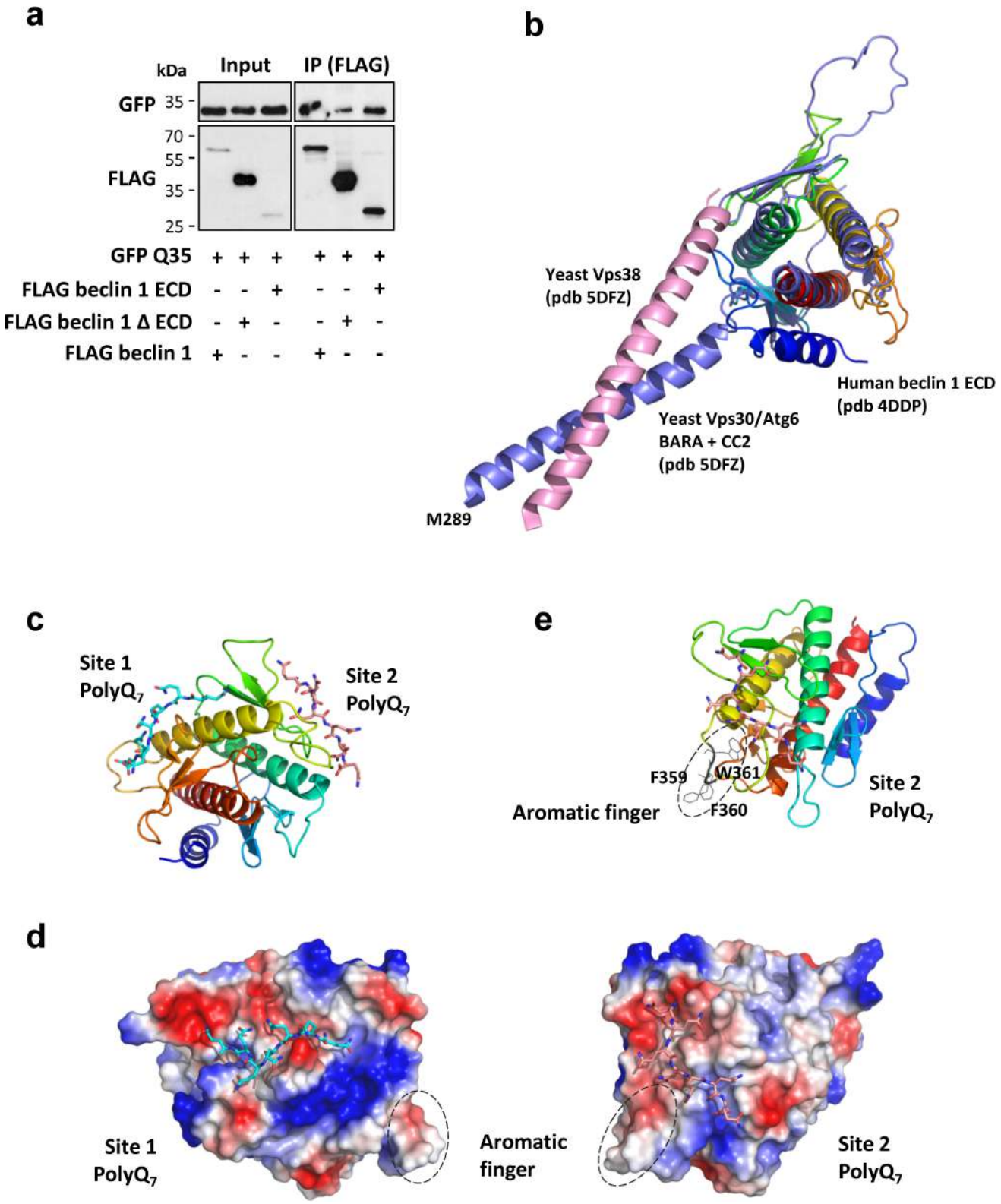

Extended Data Figure 5 | Analysis of the interaction of the polyQ domain with beclin 1. a, Flag–beclin 1 ECD alone, Flag–beclin 1 ΔECD, Flag–beclin 1 full length and GFP–Q35 were transfected into HeLa cells for 24 h and the cell lysates were immunoprecipitated with anti-Flag antibody. Immunocomplexes were analysed using anti-GFP antibody. **b**, Superimposition of human beclin 1 ECD (pdb 4DDP) and Vps30 (pdb 5DFZ), the yeast orthologue of beclin 1. The N-terminal helix (dark blue helix) of the human structure is displaced, probably owing to protein truncation for crystallographic purposes. The yeast structure suggests that this helix is part of the coiled-coil CC2 of beclin 1 instead of the ECD. **c**, Two binding sites in human beclin 1 ECD reveal high docking scores for $polyQ_7$ (the docking scores for site 1 and site 2 are −10.394 and −10.721, respectively). Sites comprising the region adjacent to the N-terminal helix (dark blue) were not considered for the docking. **d**, **e**, Surface charge illustrations of human beclin 1 ECD with the two sites of polyQ interaction. Site 2 is close to a protruding hydrophobic loop (aromatic finger) comprising Phe359, Phe360 and Trp361 (top right **e**, cartoon view), which are thought to be implicated in anchorage of beclin 1 to lipid membranes.

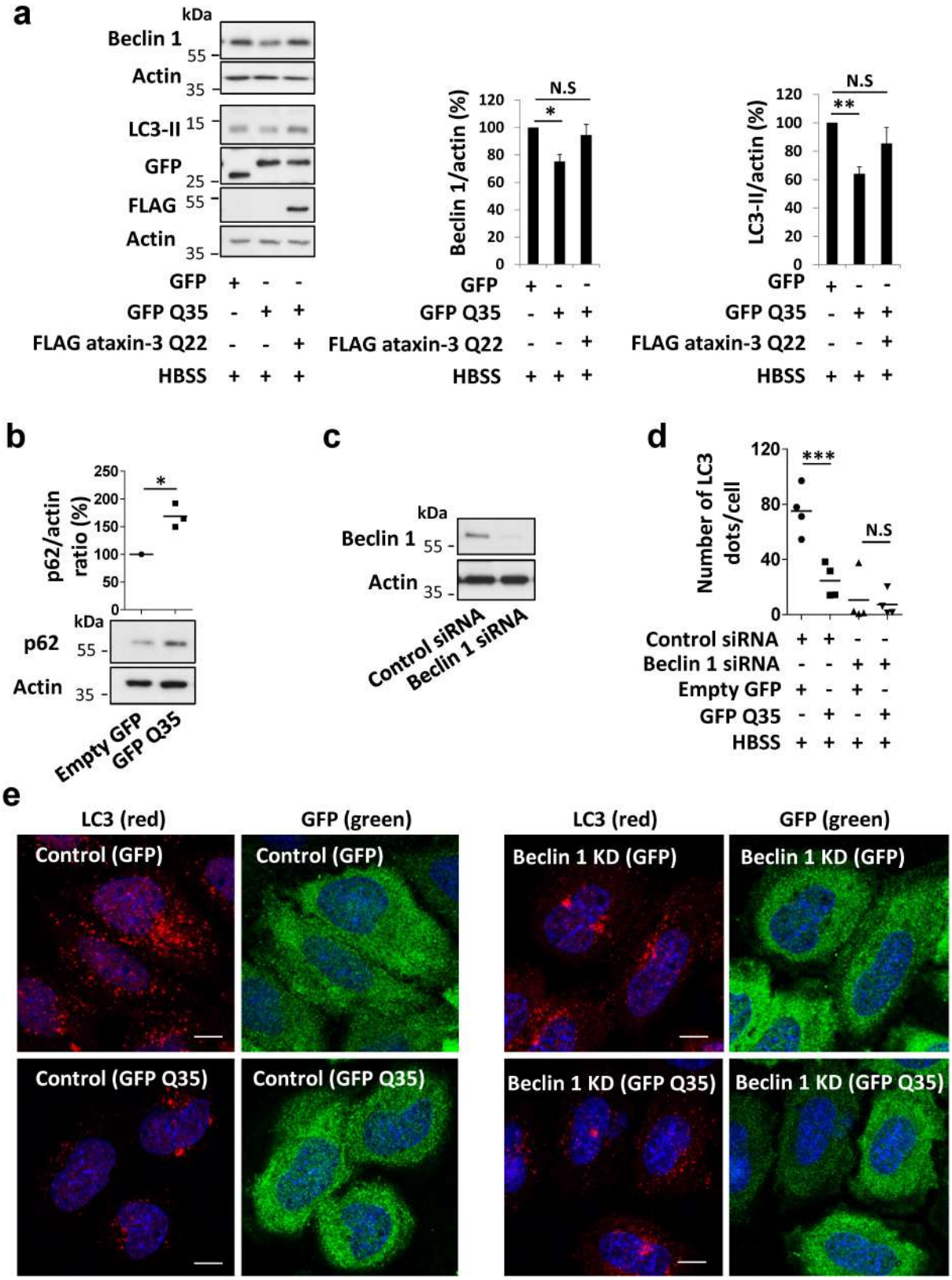

Extended Data Figure 6 | See next page for caption.

Extended Data Figure 6 | Expression of polyQ tracts impairs beclin 1-dependent starvation-induced autophagy. a, HeLa cells were transfected with empty GFP or GFP–Q35 with or without Flag–ataxin 3 Q22 for 24 h and were shifted to HBSS for the last 4 h. LC3-II and beclin 1 levels were analysed from the cell lysates. Results are mean ± s.e.m. normalized to control (empty GFP), $n = 5$ independent experiments, one-way ANOVA (for LC3-II $P < 0.01$, for beclin 1 $P < 0.05$) with post hoc Tukey's test. **b**, HeLa cells were transfected with empty GFP or GFP–Q35 for 24 h and were shifted to HBSS for the last 4 h. p62 levels were than analysed from the lysates. Results normalized to control (empty GFP), $n = 3$ independent experiments, one-tailed paired *t*-test. **c**, HeLa cells were treated with 20 nM *Becn1* siRNA or scrambled siRNA (control) for 3 days. Beclin 1 KD efficiency is presented. **d**, **e**, Control and beclin 1 KD HeLa cells were transfected with empty GFP or GFP–Q35 for 24 h and were shifted to HBSS for the last 4 h. The number of endogenous LC3 dots (red) was analysed in the GFP-expressing cells (green). Results are mean number of LC3 dots per cell in four fields from a representative experiment out of three independent experiments, as well as confocal images for each condition (number of cells analysed in control GFP $n = 32$, control GFP–Q35 $n = 27$, beclin 1 KD GFP $n = 25$, beclin 1 KD GFP–Q35 $n = 23$). Scale bars, 10 μm. Two-way ANOVA (column factor GFP Q35 $P < 0.01$, row factor beclin 1 KD $P < 0.001$, interaction $P < 0.01$) with Bonferroni's post-test. $^{*}P < 0.05$, $^{**}P < 0.01$, $^{***}P < 0.001$, NS, not significant.

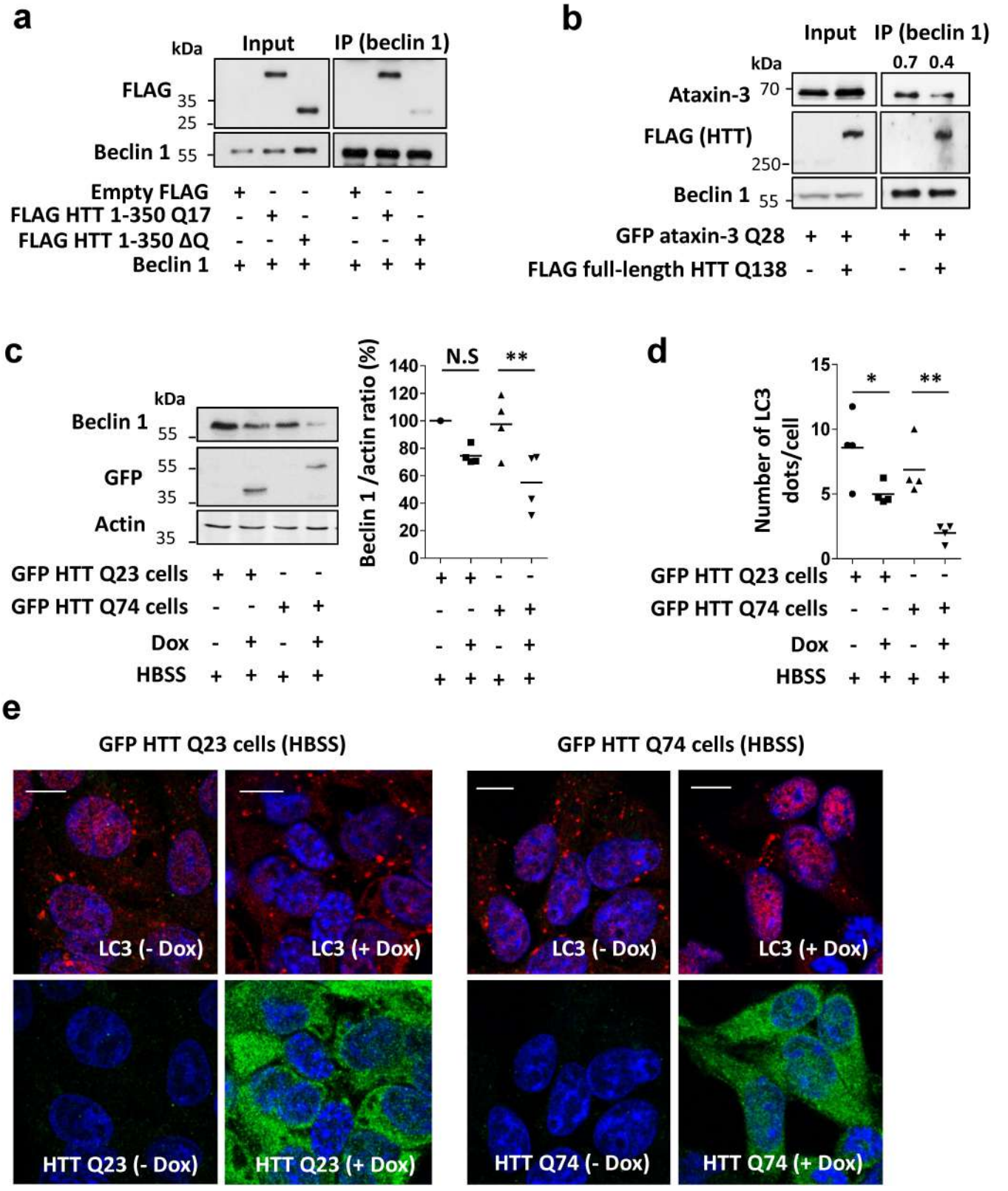

Extended Data Figure 7 | See next page for caption.

Extended Data Figure 7 | Impaired starvation-induced autophagy and reduced beclin 1 levels in cells expressing expanded polyQ forms of huntingtin. a, Empty Flag, Flag–huntingtin (HTT) N-terminal fragment (1–350) Q17, Flag–HTT (1–350) ΔQ and beclin 1 were transfected into HeLa cells for 24 h and cell lysates were immunoprecipitated with anti-beclin 1 antibody. Immunocomplexes were analysed using anti-Flag antibody. **b**, GFP–ataxin 3 Q28 and Flag–HTT Q138 (full length) were transfected into HeLa cells for 24 h and endogenous beclin 1 was immunoprecipitated. Immunocomplexes were analysed using anti-ataxin 3 antibody (detects GFP–ataxin-3) and anti-Flag antibody (detects HTT). The ratio of the bound ataxin 3 to beclin 1 is presented. **c**, Stable-inducible HEK293 cells were switched on for 48 h with doxycycline (Dox) to express GFP–HTT wild-type exon 1 (GFP–HTT Q23) or mutant GFP–HTT exon 1 (GFP–HTT Q74). In the last 4 h cells were starved (HBSS) and beclin 1 levels were analysed in each cell type. Results are normalized to control HTT Q23 cells with no Dox ($n = 4$ independent experiments). Two-way ANOVA (column factor Dox $P < 0.01$, row factor HEK 293 cells NS, interaction NS) with Bonferroni's post-test. **d**, **e**, Quantification of the number of LC3 dots in the starved cells. Results are mean dots per cell in four fields of a representative experiment out of three independent experiments. Representative confocal images of endogenous LC3 dots (red) and GFP–HTT (green) in each of the conditions (number of cells analysed in GFP–HTT Q23 no Dox $n = 41$; GFP–HTT Q23 with Dox $n = 34$; GFP–HTT Q74 no Dox $n = 39$; GFP–HTT Q74 with Dox $n = 43$). Scale bars, 10 μm. Two-way ANOVA (column factor Dox $P < 0.001$, row factor HEK cells $P < 0.05$, interaction NS) with Bonferroni's post-test. $^{*}P < 0.05$, $^{**}P < 0.01$, NS, not significant.

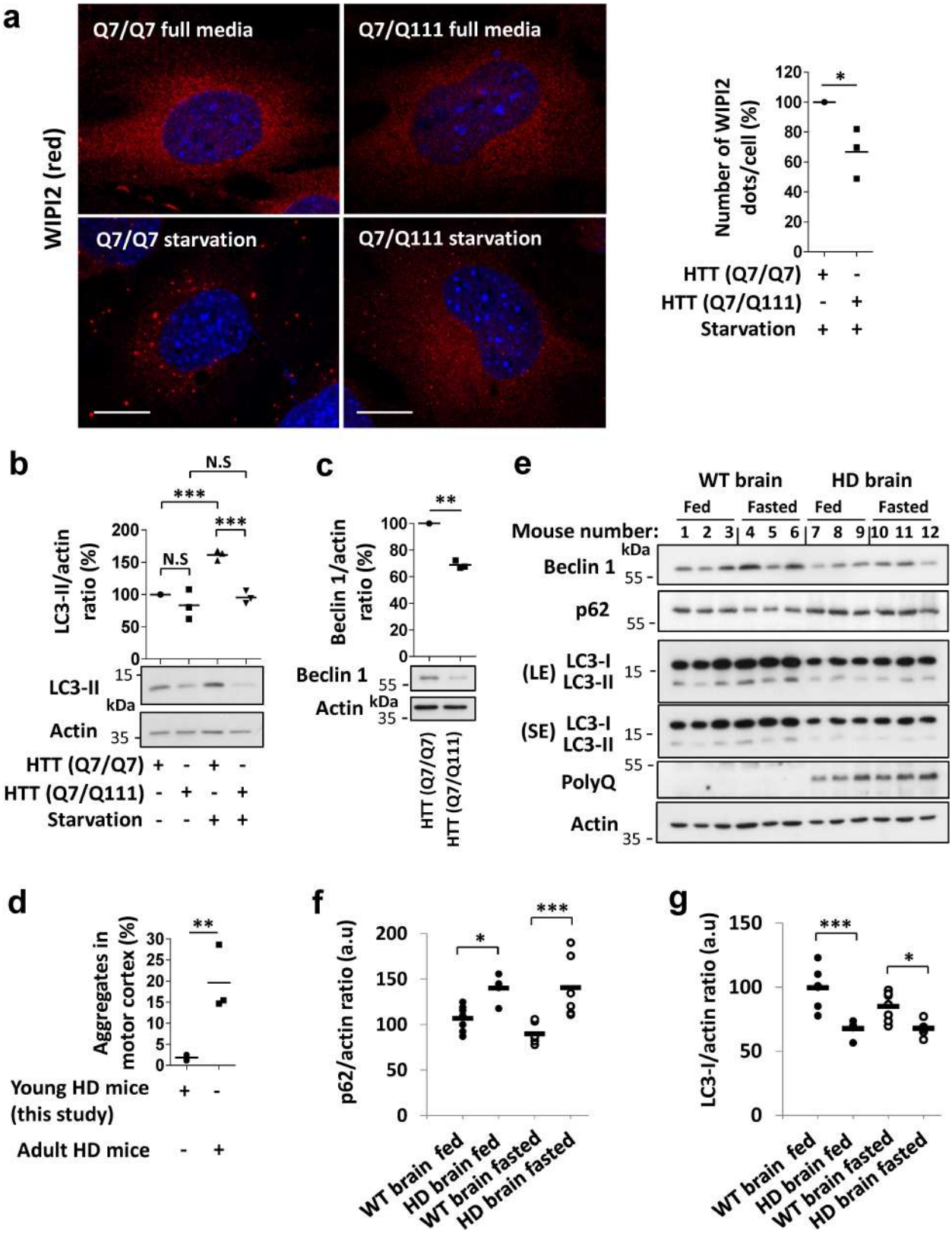

Extended Data Figure 8 | See next page for caption.

Extended Data Figure 8 | Impaired starvation-induced autophagy in striatal cell lines and in brain tissue from mouse models of Huntington's disease. a, Striatum-derived cells from HTT (Q7/Q111) heterozygous knock-in mouse and HTT (Q7/Q7) wild-type knock-in mouse were kept in full medium or starved (EBSS, 1 h). In each experiment, cells were analysed for WIPI2 dots under different conditions. We could not detect WIPI2 dots in full medium in these cells as dots became apparent after starvation-induced autophagy. The number of WIPI2 dots per cell is normalized to control HTT (Q7/Q7) cells. $n = 3$ independent experiments, one-tailed paired *t*-test. Representative confocal images of WIPI2 (red) in each of the conditions are presented ($n = 80$ cells analysed). Scale bars, 10 μm. **b**, HTT (Q7/Q111) and HTT (Q7/Q7) striatal cells were treated with BafA1 (400 nM) in full medium or starved with HBSS together with BafA1 (400 nM) for 4 h and analysed for LC3-II levels. Results are normalized to control (HTT (Q7/Q7) in full medium). $n = 3$ independent experiments, two-way ANOVA (column factor mutant HTT $P < 0.001$, row factor starvation $P < 0.01$, interaction $P < 0.01$) with Bonferroni's post-test. **c**, Beclin 1 levels in the starved HTT (Q7/Q111) and HTT (Q7/Q7) striatal cells. Results are normalized to control HTT (Q7/Q7) cells. $n = 3$ independent experiments. One-tailed paired *t*-test. **d**, Sections of brains from HD-N171-N82Q transgenic young and adult mice (6 and 12 weeks old, respectively) were analysed for neuronal aggregates in the motor cortex. For each brain, 400 cells were counted in at least three sections. Results are mean percentage of cells with aggregates from three brains, one-tailed unpaired *t*-test. **e**, Young wild-type (WT) mice and HD transgenic mice were fed or fasted. Brains from these mice were dissected and homogenized, and proteins were resolved by SDS–PAGE to analyse the levels of endogenous beclin 1, LC3-I, LC3-II and p62. PolyQ levels were analysed using anti-polyQ antibody showing the expression level of the polyQ HTT exon 1. Representative blots are shown that were used to generate the data in Fig. 4c, d. **f**, **g**, Quantification of p62 and LC3-I levels in each group (WT fed $n = 7$, HD fed $n = 5$, WT fasted $n = 7$, HD fasted $n = 6$). For LC3-I levels, two-way ANOVA (column factor HD $P < 0.001$, row factor fasting NS, interaction NS) with Bonferroni's post-test. For p62 levels, two-way ANOVA (column factor HD $P < 0.001$, row factor fasting NS, interaction NS) with Bonferroni's post-test. $^{*}P < 0.05$, $^{**}P < 0.01$, $^{***}P < 0.001$, NS, not significant.

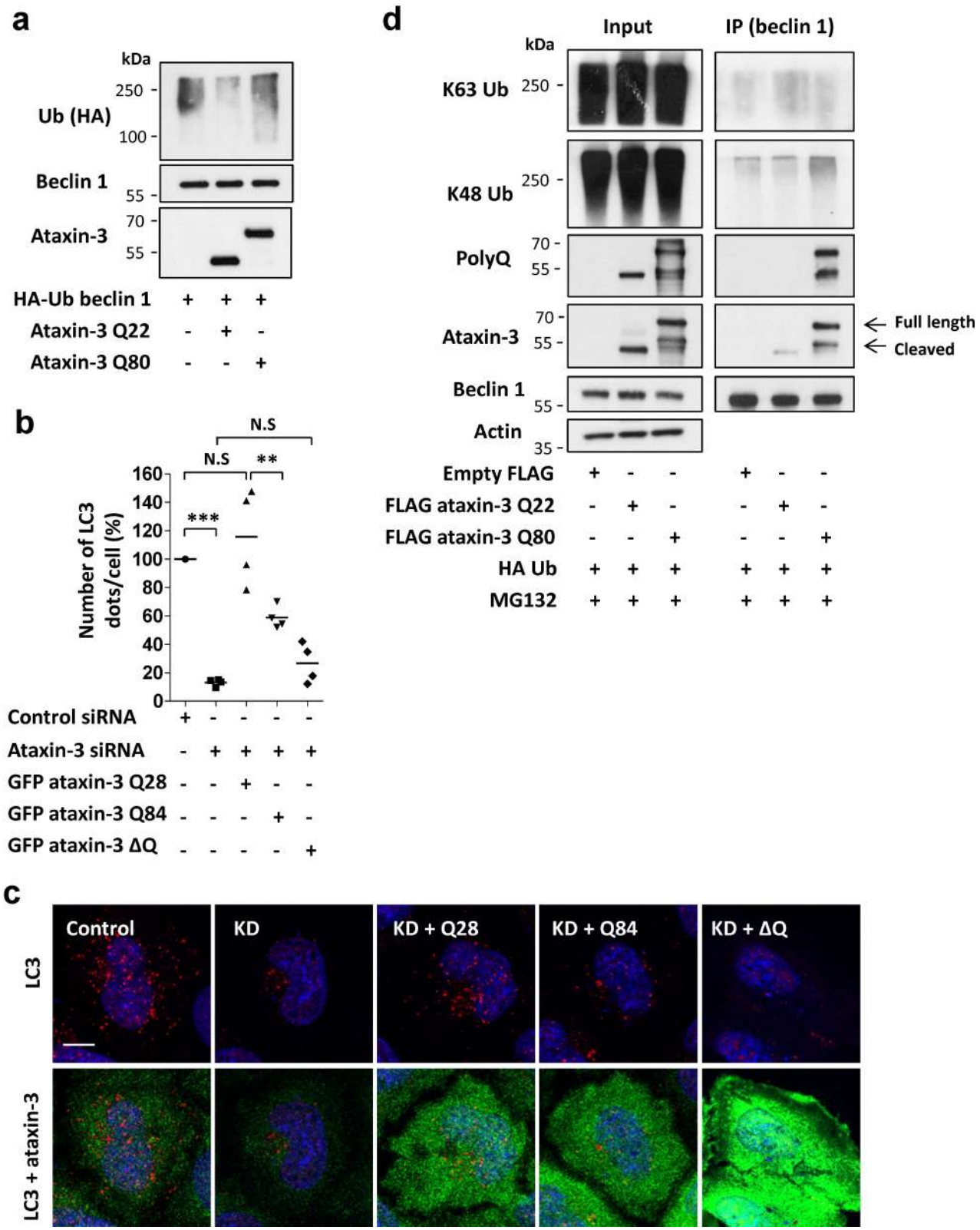

Extended Data Figure 9 | Expansion of the polyQ domain in ataxin 3 decreased deubiquitinase activity and increased interaction with beclin 1. a, Beclin 1 was purified from proteasome inhibitor-treated cells that co-expressed HA–Ub and was incubated *in vitro* with recombinant ataxin 3 Q22 or ataxin 3 Q80 for 30 min in deubiquitination buffer. Samples were analysed for beclin 1 ubiquitination using anti-HA antibodies. **b**, Number of LC3 dots in ataxin 3 KD HeLa cells that were transfected with GFP–ataxin 3 Q28, GFP–ataxin 3 Q84 or GFP–ataxin 3 ΔQ and starved with HBSS for the last 4 h. Results are normalized to control siRNA-treated cells from $n = 4$ independent experiments. One-way ANOVA ($P < 0.001$) with post hoc Tukey's test. **c**, Representative confocal images are presented for each of the conditions from **b** (LC3 dots in red and ataxin-3 staining in green, $n = 20$ cells analysed). Scale bar, 10 μm. **d**, HeLa cells were transfected with empty vector, Flag–ataxin 3 Q22, Flag–ataxin 3 Q80 and HA–Ub for 24 h and treated for the last 6 h with MG132 (10 μM). Endogenous beclin 1 was immunoprecipitated from the lysates for analysis of different polyUb linkages using K48 polyUb or K63 polyUb antibodies, and for detection of bound ataxin 3 using anti-ataxin 3 and anti-polyQ antibodies. $^{**}P < 0.01$, $^{***}P < 0.001$, NS, not significant.

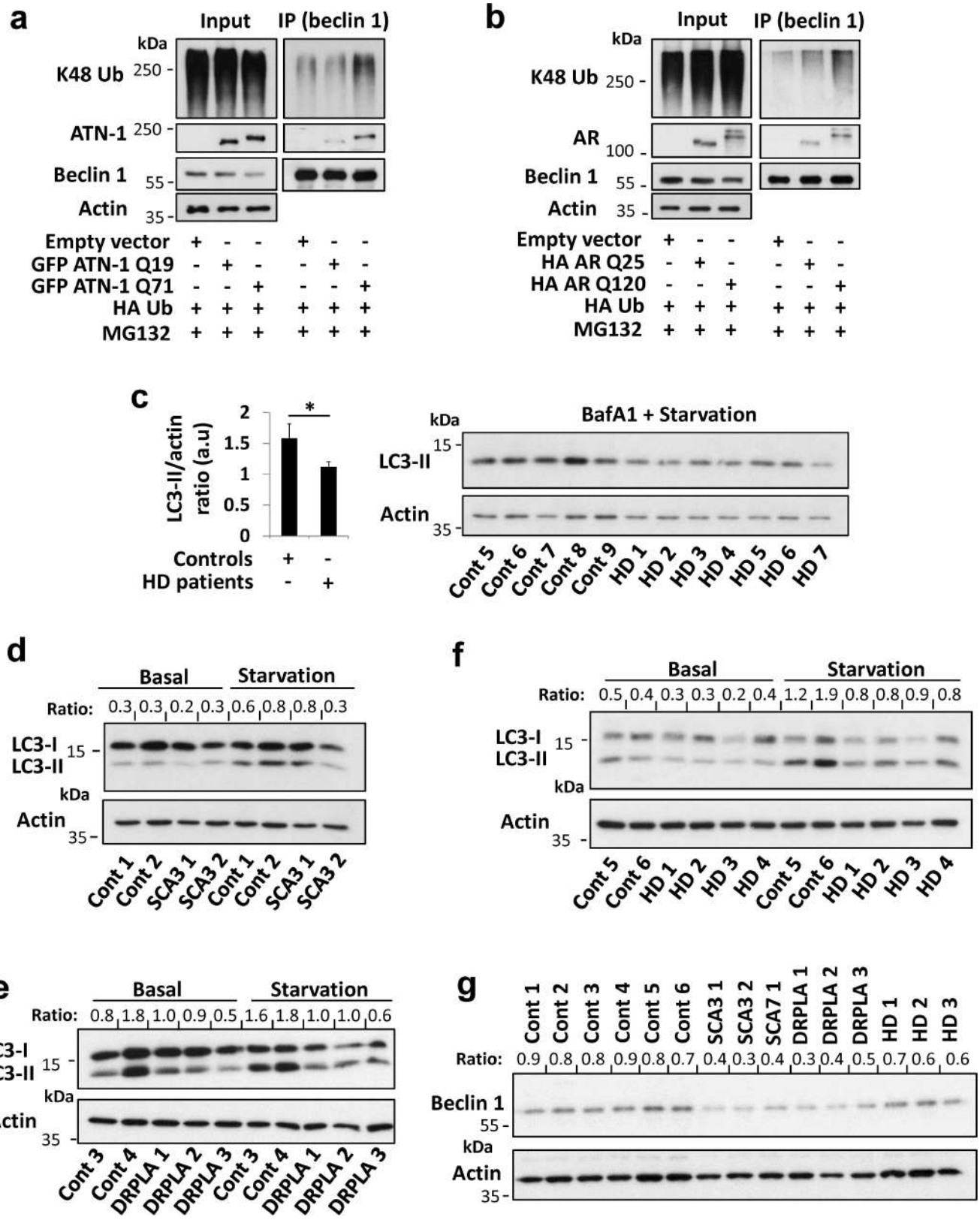

Extended Data Figure 10 | See next page for caption.

Extended Data Figure 10 | Effect of different disease proteins with polyQ expansion on beclin 1 ubiquitination, beclin 1 levels and starvation-induced autophagy. a, HeLa cells were transfected with empty vector, GFP–atrophin 1 (ATN-1) Q19, or GFP–ATN-1 Q71 along with HA–Ub for 24 h and treated for the last 6 h with MG132 (10 μM). Endogenous beclin 1 was immunoprecipitated from the lysates for ubiquitination analysis and for detection of bound ATN-1 using anti-ATN-1 antibody. **b**, HeLa cells were transfected with empty vector, HA–androgen receptor (AR) Q25, or HA–AR Q120 along with HA–Ub for 24 h and treated for the last 6 h with MG132 (10 μM). Endogenous beclin 1 was immunoprecipitated from the lysates for ubiquitination analysis and for detection of bound AR using anti-AR antibody. **c**, Primary fibroblasts derived from healthy controls (Cont) ($n = 5$) and from patients with Huntington's disease (HD) ($n = 7$) were starved with HBSS together with BafA1 (400 nM) for 4 h and analysed for LC3-II levels. Results are mean ± s.e.m. $^*P < 0.05$, one-tailed Mann–Whitney test. **d**–**f**, Primary fibroblasts derived from healthy controls and from patients with different polyQ diseases (**d**, SCA3; **e**, DRPLA; **f**, Huntington's disease) were kept in full medium or starved with HBSS for 4 h and analysed for LC3-II levels (LC3-II/actin ratio is presented). The BafA1 experiments for these sets of patients are presented in Fig. 4. **g**, Beclin 1 levels (beclin 1/actin ratio is presented) in the starved control cells compared to cells from patients with SCA3, SCA7, DRPLA or Huntington's disease. We only had one SCA7 patient sample and thus we have not analysed it further.